AGU PUBLICATIONS

Water Resources Research

RESEARCH ARTICLE
10.1002/2017WR020604

Sediment Transport of Fine Sand to Fine Gravel on Transverse Bed Slopes in Rotating Annular Flume Experiments

Anne W. Baar[1], Jaco de Smit[1,2], Wim S. J. Uijttewaal[3], and Maarten G. Kleinhans[1]

[1]Faculty of Geosciences, Universiteit Utrecht, Utrecht, the Netherlands, [2]Department of Estuarine and Delta Systems, NIOZ Royal Netherlands Institute for Sea Research, Yerseke, the Netherlands, [3]Faculty of Civil Engineering and Geosciences, Delft University of Technology, Delft, the Netherlands

Key Points:
- Transverse slope effects are quantified for a large range in helical flow intensity and sediment mobility using a rotating annular flume
- The resulting trend in slope effect deviates from typical power relations with Shields number and is grainsize-dependent
- The relatively low slope effects are in contrast with the tendency to increase slope effects in current morphodynamic models

Supporting Information:
- Supporting Information S1
- Data Set S1

Correspondence to:
A. W. Baar,
A.W.Baar@uu.nl

Citation:
Baar, A. W., de Smit, J., Uijttewaal, W. S. J., & Kleinhans, M. G. (2018). Sediment transport of fine sand to fine gravel on transverse bed slopes in rotating annular flume experiments. *Water Resources Research*, *54*, 19–45. https://doi.org/10.1002/2017WR020604

Received 16 FEB 2017
Accepted 17 DEC 2017
Accepted article online 21 DEC 2017
Published online 4 JAN 2018

Abstract Large-scale morphology, in particular meander bend depth, bar dimensions, and bifurcation dynamics, are greatly affected by the deflection of sediment transport on transverse bed slopes due to gravity and by secondary flows. Overestimating the transverse bed slope effect in morphodynamic models leads to flattening of the morphology, while underestimating leads to unrealistically steep bars and banks and a higher braiding index downstream. However, existing transverse bed slope predictors are based on a small set of experiments with a minor range of flow conditions and sediment sizes, and in practice models are calibrated on measured morphology. The objective of this research is to experimentally quantify the transverse bed slope effect for a large range of near-bed flow conditions with varying secondary flow intensity, sediment sizes (0.17–4 mm), sediment transport mode, and bed state to test existing predictors. We conducted over 200 experiments in a rotating annular flume with counterrotating floor, which allows control of the secondary flow intensity separate from the streamwise flow velocity. Flow velocity vectors were determined with a calibrated analytical model accounting for rough bed conditions. We isolated separate effects of all important parameters on the transverse slope. Resulting equilibrium transverse slopes show a clear trend with varying sediment mobilities and secondary flow intensities that deviate from known predictors depending on Shields number, and strongly depend on bed state and sediment transport mode. Fitted functions are provided for application in morphodynamic modeling.

1. Introduction

Subaqueous morphology arises from the interaction of flow and sediment transport. Starting from minor perturbations, the nonlinear dependence of sediment transport rate on flow shear stress at the bed causes growth of bedforms and bars, as deeper channels attract more flow, causing much more sediment transport, and the reverse for shallower areas. An important negative feedback on vertical growth is the direct pull by gravity on particles moving on gently sloping beds. Large-scale morphology in all aqueous environments with movable bed sediment is greatly affected by this. In particular, the bed slope effect determines wavelengths of coastal sandbanks and sand waves (Blondeaux & Vittori, 2016; Hulscher, 1996), steepness of surf zone bars formed by gravity waves (Ruessink et al., 2007), length of fluvial bars and braiding index (Crosato & Mosselman, 2009; Struiksma et al., 1985), properties of tidal bars (Leuven et al., 2016; Schramkowski et al., 2002; Seminara & Turbino, 2001), and estuarine braiding (Van der Wegen & Roelvink, 2012), and stability of river bifurcations (Bolla Pittaluga et al., 2015).

Here we focus on this transverse bed slope effect in curved channels with unidirectional flow and uniform sediment. In a straight river section, the fluid drag on sediment particles is generally directed downstream along the river, while the bed slope, usually the largest in transverse direction, causes sediment particles to also travel downslope across the channel. The net effect is an angle between the direction of sediment transport and the mean flow direction. The typical transverse slope that develops here is a balance between the shear stress in downstream direction and sediment properties that determine the gravity component in the transverse direction (e.g., Sekine & Parker, 1992; Talmon et al., 1995; Van Bendegom, 1947). This is further modified by secondary flow patterns induced by bars and bends. These secondary currents alter the direction of the bed shear stress towards the inner bend. This leads to an equilibrium transverse slope toward the inner bend when the downslope gravitational force on particles is balanced by the upslope directed drag force by secondary flow (Figure 1) (e.g., Engelund, 1974; Struiksma et al., 1985).

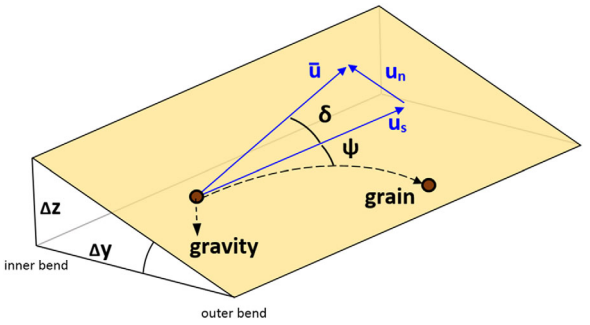

Figure 1. Definition of the main variables that determine the transverse bed slope effect. Grains on a slope transverse to the main flow direction (u_s) are deflected downslope due to gravity. When a secondary current is present, e.g., in bends, the inward and upslope directed shear stress drags particles upslope. In this case the equilibrium slope that develops ($\frac{\partial z_b}{\partial y}$) is a balance between the angle of deflection due to gravity (ψ) and the angle between the local flow velocity vector ($\vec{u}$) and the main flow direction (δ) near the bed, which represents the secondary flow intensity (after Schuurman, 2015; Sekine & Parker, 1992).

The transverse bed slope effect strongly influences bar patterns. Locally, slope effects determine bar height and active channel width (Schuurman et al., 2013). For example, a strong bed slope effect, i.e., a large deflection of sediment downslope, leads to low and wide bars. On a larger-scale, transverse bed slope effects influence the adaptation of the bed to perturbations in the flow, as secondary currents are balanced by the transverse bed slope effect. The secondary flow patterns and the corresponding transverse bed slope do not appear instantaneously downstream of the bend entry, but adapt asymptotically (Struiksma et al., 1985). A strong bed slope effect causes the bend to adapt to an equilibrium slope over a relatively short reach and bars have the tendency to disappear within a short distance downstream, whereas weaker transverse bed slope effects allow perturbations to propagate further downstream (Crosato & Mosselman, 2009; Kleinhans & van den Berg, 2011). This process is illustrated by Van der Wegen and Roelvink (2012) and Schuurman et al. (2013), who tested the sensitivity of a sandy estuary and of a morphodynamic model of a braided sand-bed river to the transverse bed slope effect. They showed that overestimating this effect leads to flattening of the morphology, while underestimating leads to unrealistically steep bars and banks and a higher braiding index downstream. An incorrect setting thus has major consequences for the predicted large-scale morphology, bank protection works, and dredging volumes for fairway maintenance (Schuurman et al., 2013; Van der Wegen & Roelvink, 2012).

The stability of bifurcations is also highly sensitive to the bed slope effect. Just upstream of the bifurcation, a transverse slope also develops as a result of a bed level difference between the distributaries, which develops when one of the branches aggradates while the other erodes. The distribution of sediment over the branches is influenced by the direction of sediment transport on this transverse slope, which affects the further development of the bifurcation (Bolla Pittaluga et al., 2003, 2015; Kleinhans et al., 2008; Sloff & Mosselman, 2012). Whether a bifurcation is stable depends on whether the sediment transport capacity difference between the downstream branches is balanced by sediment transport in downslope direction feeding into the deeper channel. The societal relevance is that bifurcations divide water, sediment, and thus flood risk over fluvial plains and deltas.

The literature reports starkly different magnitudes of the bed slope effect. Previous studies isolated a specific transport mechanism or bed state and study its separate effect on the transverse bed slope effect. Consequently, the resulting predictors are based on a small set of experiments, with a maximum of 11 unique experiments (Talmon et al., 1995) and a minor range of flow conditions and sediment sizes depending on the process that is studied (e.g., Ikeda & Nishimura, 1986; Struiksma et al., 1985; Talmon & Wiesemann, 2006). However, these predictors are now used in numerical morphodynamic modeling where all processes act in combination. As a result, current models often overpredict channel depth and bar height, so that the transverse bed slope parameters in current models in practice need to be calibrated on measured morphology. This means that the most important results of morphological models depend critically on a poorly quantified parameter representing a poorly understood combination of processes. Unfortunately, calibrating morphology on bed slope parameters also compensates for other model weaknesses such as poorly parameterized or absent processes, e.g., bank erosion, bed form effects on sediment transport and flow resistance. To some degree, calibration parameters account for the effect of sediment mobility and transport mode (rolling or saltating bed load to sheet flow), presence of bedforms of different types (ripples and dunes) with strong subgrid variations in transverse and streamwise slopes, and transverse sediment sorting effects, such as the classic bend sorting (Sekine & Parker, 1992; Wiesemann et al., 2006). To test whether poor model behavior and the need for calibration beyond expected parameter ranges is caused by poor bed slope predictors or other model issues, we urgently need a comprehensive set of data for a large range of sediment mobility and grainsize, covering all sediment transport modes and bed state regimes. The key problem is the scarcity of experimental data covering all these processes to test and calibrate process-specific transverse bed slope relations.

The objective of this research is to experimentally quantify the transverse bed slope effect for a large range of near-bed flow conditions and sediment sizes to obtain parameters for morphological modeling that cover all sediment transport modes and bed state regimes. We conducted experiments with a set of sediments in a rotating annular flume, which allows control of the secondary flow intensity independently from the streamwise flow velocity. Therefore, all important parameters could be isolated and their separate effect on the transverse slope can be determined. Below we first review transverse bed slope predictors and their limitations, followed by a description of our experimental setup, data reduction of the 224 experiments conducted in fine sand to fine gravel, and finally discuss the results and draw conclusions.

2. Existing Transverse Slope Predictors

An inclination of the bed in streamwise as well as transverse direction affects the magnitude of sediment transport, and additionally a transverse slope causes a deviation of the direction of the transport vector from the applied bed shear stress (Francalanci et al., 2009; Parker et al., 2003). Furthermore, an inclined bed lowers the critical shear stress for the beginning of motion compared to a horizontal bed (Fernandez Luque & Van Beek, 1976; Seminara et al., 2002). In this paper, we will focus on the effect of transverse slopes because these typically are orders of magnitude larger than average streamwise slopes.

The simplest relation used in literature for the change in sediment transport direction due to slope effects in transverse direction was formulated for river bends by Van Bendegom (1947) as:

$$tan(\psi) = tan(\delta) - \frac{1}{B}\frac{\partial z_b}{\partial y} \tag{1}$$

where ψ = direction of sediment transport, δ = direction of near-bed flow velocity, affected the intensity of the secondary current, and B = a dimensionless slope factor. See Figure 1 for definition of parameters. This equation shows that the secondary flow intensity, which is directed upslope in curved channel sections, counteracts slope effects. Consequently, when equilibrium is attained in an infinitely long bend of constant curvature because net transverse sediment transport is zero, this equation reduces to a balance:

$$\frac{\partial z_b}{\partial y} = Btan(\delta) = B\frac{u_n}{u_s} \tag{2}$$

where u = magnitude of the flow velocity (m/s) in transverse direction (n) and streamwise direction (s). A later refinement of this linear relation between the secondary flow intensity and the transverse slope is the nonlinear model of Parker et al. (2003), in which the slope factor itself depends on the transverse slope. Francalanci and Solari (2008) approximated the nonlinear equation of Parker et al. (2003) with polynomial functions of the local transverse bed slope, which was tested experimentally together with the linear model of Parker et al. (2003) by Francalanci et al. (2009). Results suggested that linear transverse bed slope predictors lead to an underestimation of lateral sediment transport.

Current transverse bed slope predictors are either based on theoretical model studies validated with laboratory experiments or field data (e.g., Engelund, 1974; Ikeda, 1984; Koch & Flokstra, 1981), or are based on an empirical fit through experimental data (e.g., Talmon et al., 1995; Wiesemann et al., 2006). Important differences between these studies relate to the factors included in the bed slope factor B. Theoretical models follow the reasoning of Van Bendegom (1947), and base the slope factor on the radial balance of forces acting on a grain moving on a transverse inclined bed. These forces consist of gravity pulling the particles downslope, a drag force on the particles in the direction of the bed shear stress, and friction between the particles and the bed (Engelund, 1974; Koch & Flokstra, 1981; Van Bendegom, 1947). The frictional forces can consist of both dynamic friction between moving particles and the bed, and static friction between nonmoving particles in the bed, which is frequently expressed as the angle of internal friction or angle of repose (Parker et al., 2003).

Table 1 lists variations of the slope factor B. The variations broadly fall into four categories. First, since the slope factor is assumed to be a function of sediment properties and fluid drag, in most studies B is a function of sediment mobility (θ) (Talmon et al., 1995). Accordingly, the slope factor is often defined in the generalized form:

Table 1
Transverse Slope Predictors and the Experimental Conditions for Which They Were Determined

Author	B	α/α_c	β	Flume	Runs (nr)	D_{50} (mm)	θ	Transport mode	Bed state	c.p. (range)
Independent of sediment mobility										
Engelund (1974)	μ_d	0.51	0	Bended	2	0.3	0.28, 0.40	Bed load	Dunes	μ_d
Engelund (1975)	μ_d	0.47	0	Annular	2	3 ($\rho = 1{,}400$)	0.25,0.75	Bed load	Lower plane bed	μ_d
Dependent on sediment mobility										
Koch and Flokstra (1981)	$\frac{3}{2}\theta f_b$	1.5	1	Bended	3	0.21, 0.78	0.67, 0.34		Ripples	$f_b(\sim 1)$
Struiksma et al. (1985)	$f_s\theta$	1	1	Bended	6	0.3–0.78	0.16–0.52	Bed load	Dunes	f_s (0.4–1.5)
Talmon et al. (1995)	$9\left(\frac{D_{50}}{H}\right)^{0.3}\sqrt{\theta}$	1.7	0.5	Straight	11	0.09–0.78	0.1–0.8	Bed load, suspended	Dunes, ripples	
Wiesemann et al. (2006)	Ripples: $\sqrt{\theta}$	1	0.5	Straight	3	0.25,0.96	0.16–0.5	Bed load, suspended	Dunes, ripples	
	Dunes: 0.9	0.9	0							
Including critical sediment mobility										
Hasegawa (1981)	$\sqrt{\frac{\mu_s\mu_d\theta}{\theta_c}}$	0.67	0.5	Straight	9	0.425	0.05–0.3		Lower plane bed	
Ikeda (1984)	$\frac{\mu_d}{1+\gamma\mu_d}\sqrt{\frac{\theta}{\theta_c}}$	0.31	0.5	Straight	2	0.18, 0.42	0.23, 0.10		Dunes	
Ikeda and Nishimura (1986)	$\frac{f_{sh}\mu_d}{1+\gamma\mu_d}\sqrt{\frac{\theta}{\theta_c}}$	0.19	0.5	Bended	1	0.15	0.3	Suspended	Ripples	$f_{sh}(\sim 0.59)$
Sekine and Parker (1992)	$1.33\left(\frac{\theta}{\theta_c}\right)^{0.25}$	1.33	0.25	Straight	11	0.425, 1.3	<0.2	Bed load (saltation)	Lower plane bed	
Parker et al. (2003)	$\frac{1}{\lambda}\sqrt{\frac{\theta}{\theta_c}}$	1.43	0.5	Straight	5	1.5–3.3	Low	Bed load (saltation)		
Talmon and Wiesemann (2006)	$\frac{\mu_d}{f_b}\sqrt{\frac{\theta}{\theta_c}}$	0.27	0.5	Straight	6	0.09–0.96	0.1–0.9	Bed load, suspended	Dunes, ripples	f_b (1–1.06)
Nonlinear relation										
Francalanci et al. (2009)	$\alpha_\psi\left(\frac{\theta}{\theta_c}\right)^{\beta_\psi}$	$\alpha_\psi\left(\frac{\partial z_b}{\partial y}\right)$	$\beta_\psi\left(\frac{\partial z_b}{\partial y}\right)$	Straight	5	3 (ρ=7850)	0.03–0.12	Bed load (saltation)	Lower plane bed	$b_\psi, d_\psi, h_\psi, m_\psi$

Note. c.p. = study-specific calibration parameter, of which the range is determined when validating the predictor with experiments.

$$B=\alpha\theta^{\beta}, \tag{3}$$

or when the critical shear stress (θ_c) is included:

$$B=\alpha_c\left(\frac{\theta}{\theta_c}\right)^{\beta} \tag{4}$$

Where the sediment mobility θ, a dimensionless form of the bed shear stress, reads:

$$\theta=\frac{\tau}{(\rho_s-\rho)gD_{50}} \tag{5}$$

where τ = shear stress (N/m^2), ρ_s = specific density of the sediment, g = gravitational acceleration (m/s^2), and D_{50} = median grainsize (m). Table 1 shows that β varies between 0 and 1, but is usually 0.5 based on the relation between shear stress and flow velocity. Henceforth, the ratio of sediment mobility θ and critical sediment mobility θ_c will be referred to as relative sediment mobility. Several studies include a critical sediment mobility for the beginning of motion (e.g., Francalanci et al., 2009; Ikeda & Nishimura, 1986; Talmon & Wiesemann, 2006), which according to Odgaard (1981) is necessary to relate the transverse slope to bed surface characteristics, instead of only bed load properties. Parker et al. (2003) included a ratio between the critical sediment mobility for the cessation of sediment transport and for the beginning of motion (λ), which is generally below 1. Similar differences in formulation of relative and excess sediment mobility exist between sediment transport predictors, which imply that transverse bed slope relations should be formulated consistently with the sediment transport relation that is used.

Second, the dominant mode of transport determines the effective gravity acting on the grains. Sekine and Parker (1992) discuss that previous theoretical relations are only valid for rolling or sliding transport, since particles are assumed to be continuously in contact with the bed. Therefore, they propose a transverse

slope predictor that is based on a stochastic model of saltating particles, resulting in a β of 0.25. However, their resulting relation has a number of simplifications and is still only valid for small transverse slopes and a low sediment mobility, since the number of saltating particles needs to be low to avoid particle collision. When suspension is present, Talmon et al. (1995) found a slope effect that is two times larger than under bed-load dominant conditions with equal flow velocities. However, in current models suspended load is not influenced by bed slope effects (Talmon et al., 1995; Van der Wegen & Roelvink, 2012), or, alternatively, suspended load is treated as bed-load when a total load sediment transport predictor is used as in Van der Wegen and Roelvink (2012) and Schuurman et al. (2013).

Third, most studies only include a dynamic friction coefficient (μ_d) to balance the fluid drag force (Ikeda & Nishimura, 1986; Talmon & Wiesemann, 2006), and thereby ignore the effects of a lower threshold of sediment motion due to a transverse slope, which depends on static friction (μ_s) (Fernandez Luque & Van Beek, 1976; Seminara et al., 2002). Engelund (1974) even assumes a slope effect that only depends on dynamic friction and is therefore independent of flow conditions and sediment size. Consequently, he concludes this predictor is only valid for small sediment transport rates. Only the predictor of Hasegawa (1981) includes static friction directly, while the predictor of Francalanci et al. (2009) takes the friction angle into account indirectly since their experiments used for calibration were designed with steel particles with a high friction angle. The values of these friction coefficients are based on experimental findings. In the predictors of Ikeda (1984) and Ikeda and Nishimura (1986), the dynamic friction depends on a ratio of lift to drag coefficient (γ), which is also a constant. In general, linear theoretical models only apply for gentle slopes, because dynamic and static friction are constant and thereby do not depend on the magnitude of the transverse slope (Sekine & Parker, 1992; Parker et al., 2003). For higher slopes, the dynamic friction changes due to the increase in slope, and thus the equation should be nonlinear.

Fourth, validation of the theoretical models with experimental data with varying bed states and particle properties lead to the need for several calibration parameters and the adjustment of the dynamic friction coefficient. Predictors based on forces acting on the grains have grain-related calibration factors to ensure an agreement with the model, namely a shape factor of the grains (f_s) (Struiksma et al., 1985) and a sheltering coefficient (f_{sh}) (Ikeda & Nishimura, 1986). Bed state was ignored in the theoretical models. Therefore, in several experimental studies either flow conditions were chosen such that bedforms were avoided (Engelund, 1975; Hasegawa, 1981), or the presence of bedforms caused a calibration parameter for the transverse bed slope predictor (Koch & Flokstra, 1981; Talmon & Wiesemann, 2006).

Dunes in particular may have large effects that are incompletely understood. In particular, the local bed streamwise and transverse slopes vary strongly along a dune as do the flow field and flow turbulence intensity, none of which is incorporated in derivations of physics-based predictors for transverse bed slope effect. In fact, bedforms occur in almost none of the current morphodynamic models meaning that their effects on flow and sediment transport are somehow calibrated into parameters for flow resistance, sediment transport, and predictors for slope effects. Existing predictors based on an empirical fit through experimental data mainly focused on the effect of different bed states, which in the case of Wiesemann et al. (2006) lead to a different trend for a bed with ripples or with dunes, since they observed that downslope sediment transport decreased when dunes were present and became independent of sediment mobility. In contrast, Sieben and Talmon (2011) used artificial dunes to show that the slope effect is enhanced when oblique dunes are present, due to avalanching at the lee sides of the dunes. Talmon et al. (1995) manually prepared dunes based on earlier experiments, since the development of natural dunes required the same time as the duration of their bed leveling experiments. They conclude that the scale of bedforms has a significant influence on the slope factor, and this value is twice as small in the experimental setting with relatively high bedforms compared to natural rivers, but this conclusion may have been affected by the initial condition. They therefore proposed a slope factor including a ratio between the water depth and the median grain-size, to account for bed form height.

Another cause for variations in B may be the type of experimental facility used to collect calibration data (see Table 1). To validate the theoretical models or to obtain an empirical fit, past experiments were conducted in either a bended flume (e.g., Ikeda & Nishimura, 1986; Struiksma et al., 1985) or an annular flume (Engelund, 1975), or straight flumes initiated with a transversely sloped bed that relaxed to a horizontal bed (e.g., Ikeda & Nishimura, 1986; Talmon et al., 1995; Talmon & Wiesemann, 2006). Straight flumes have the advantage of reasonably isolating the transverse bed slope effect without strong bend flow, but have the

disadvantage that the transverse bed slope effect is determined from the initial changes of the disequilibrium bed slope rather than an equilibrium morphology, and that the bed state, e.g., dunes, develops at the same timescale (Talmon & Wiesemann, 2006). In curved flumes and in the annular flume of Engelund (1975), a morphodynamic equilibrium is possible, which has the advantage of straightforward measurement of the transverse bed slope but the disadvantage that this result depends on secondary flow patterns that need to be quantified and are only valid for one single bend radius. An annular flume additionally has the advantage that it avoids boundary effects and the flow does not have to adapt to changes in channel curvature, and therefore the transverse slope that develops in the flume is in equilibrium with the established flow conditions along the entire flume. This requires that the flow conditions are well known. To study the effect of different bend radii, a rotating annular flume was used in the current research, in which the intensity of the secondary flow can be controlled and varied by counterrotating the floor and side walls of the flume (Booij, 2003). Thereby, the effect of the secondary flow can be isolated by simulating infinite bends with various bend radii. This concept will be explained in more detail in the next section.

The need to develop experiments with appropriate conditions for testing certain predictors led in practice to limited experimental data sets. In the case of validation of a theoretical model, the conditions were chosen such that they fit the model assumptions, for instance absence of bed forms. As a result, all experiments reported so far were performed with a limited range in flow conditions and sediment sizes depending on the studied process, with a maximum of 11 unique experimental settings (Table 1). As a side effect, the effects of varying bed states and sediment transport modes on slope effects were mostly ignored in past studies. Consequently, the amount of data to test and calibrate transverse bed slope relations is too scarce and inconsistent.

Estimates of the magnitude of the transverse slope factors α or α_c and β in equation (3) are given in Table 1, based on reported theoretical and calibration parameters by the corresponding studies. The range of α varies between 0.47 and 1.7, and is comparable with the range of α_c, which varies between 0.19 and 1.43. These ranges comprise constant values typically used in morphodynamic models, and consequently transverse slope factors are linearly related to sediment mobility throughout a model run. Even though the magnitudes of the transverse slope factors were validated for a specific process and corresponding range in flow conditions and sediment mobility, current morphodynamic models apply these values in a wide range of environments and conditions. We illustrate the problems that arise in applications here with the implementation of bed slope effects in the state-of-the-art morphodynamic model Delft3D. Typically, a predictor based on either Koch and Flokstra (1981) or Ikeda (1984) is used to calculate bed load transport on transverse slopes, with the main difference that in the predictor of Ikeda (1984) a critical shear stress is used, which is absent in the predictor of Koch and Flokstra (1981). However, the resulting transport vector is calculated in different ways for these predictors. First, the magnitude of sediment transport is predicted, based on a situation of a flat bed with a single grainsize. Second, for Koch and Flokstra (1981) the direction of sediment transport is corrected for transverse gradients by rotating the transport vector:

$$tan(\psi) = \frac{1}{\alpha\theta^{\beta}} \frac{\partial z_b}{\partial y} \tag{6}$$

On the other hand, for Ikeda (1984) an additional transport vector is calculated perpendicular to the flow direction (Van der Wegen & Roelvink, 2012; Van Rijn, 1993):

$$q_n = q_s \frac{1}{\alpha_c} \sqrt{\frac{\theta_c}{\theta}} \frac{\partial z_b}{\partial y} \tag{7}$$

where q = sediment transport load (m^2/s). α, β, and α_c are user-defined adjustable parameters. Here the default value of α in Delft3D is set to 1.5, which is directly taken from Koch and Flokstra (1981). β_k is set to 0.5, which differs from the value of 1 proposed by Koch and Flokstra (1981), but is equivalent to most other predictors (Table 1). Schuurman et al. (2013) varied α between 0.35 and 1.5 and eventually used a value of 0.7. Based on the experiments of Ikeda (1984) in a straight flume, Van Rijn (1993) concluded α_c should be around 0.67, which is thus the default value for the second bed slope option in Delft3D. Details on the default values for both α and α_c, and how compare them are given in Appendix B. However, in practice both slope factors are reduced to 1 or 2 orders of magnitude smaller than the default values in the calibration to measured morphology, to correct for the tendency of the model to overdeepen channels and

exaggerate bar length (e.g., Schuurman et al., 2013; Van der Wegen & Roelvink, 2012), and the absence of physics-based bank erosion (e.g., Grenfell, 2012; Schuurman et al., 2013). For example, the modeled braided sand-bed river of Schuurman et al. (2013) showed an increase of more than 60% in channel depth and an increase in braiding index from 2.4 to 3.5 after 25 months when using his optimal value of 0.7 for α compared to a model run with the lower value of 0.35. They therefore concluded that the model results are very sensitive to a change in this parameter value. The study of Van der Wegen and Roelvink (2012) compared two model runs based on an existing morphology of a sandy estuary with an α_c of 0.1 and 0.2, which showed an increase of 8% in channel depth and a higher braiding index than the morphology when using the higher value despite the fact that this is still significantly lower than the default value of 0.67. This sensitivity of predicted long-term morphology to the transverse bed slope parameters, even when a measured bathymetry is used for calibration, illustrates the need for a better understanding of the transverse bed slope effect.

3. Methods

3.1. Experimental Methodology

We conducted experiments in a rotating annular flume (Figure 2) which allows control of the secondary flow intensity independently from the streamwise flow velocity. Rotation of the flume lid drives the flow by applying a shear stress on top of the water column. This not only generates streamwise flow, but also causes a secondary circulation to develop due to the curvature of the flume. The centrifugal force generated by rotating the lid causes water to be pushed outward at the top of the water column which creates a pressure gradient from the outer to the inner bend. This pressure gradient drives the secondary flow and thereby creates an inward-directed bed shear stress near the bed, which corresponds with the development of secondary flow patterns in natural river bends. However, in a rotating annular flume the secondary flow can be counteracted by rotating the floor of the flume plus attached sidewalls in opposite direction. By counterrotating the floor, an outward-directed centrifugal force is added on the flow low in the water column, which decreases the pressure difference over the water column at the outer bend, and thereby decreases the secondary flow and the inward-directed bed shear stress (Booij, 1994, 2003). Both the lid and floor of the flume can rotate over a continuous range of angular velocities in both directions. By controlling lid and floor angular velocities, the streamwise flow velocity as well as the secondary flow can be isolated and thus the ratio between these parameters can be varied as well. Changing this ratio alters the direction of the flow velocity vector near the bed, which determines the secondary flow intensity and corresponds to different bend radii in nature. Most studies until now (e.g., Booij, 1994; Yang et al., 2015) sought the ratio of

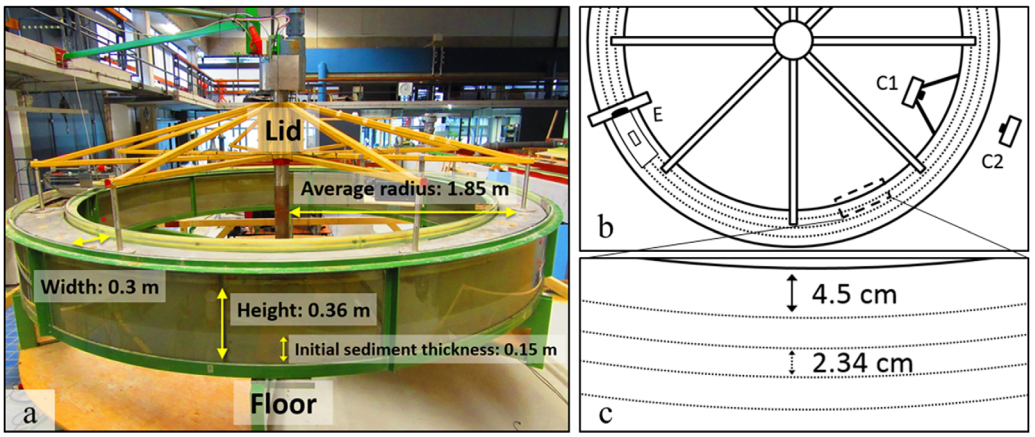

Figure 2. Experimental setup. (a) The dimensions of the rotating annular flume. Floor and sidewalls are attached; lid rotates independently. (b; top view) Schematic drawing of the measurement setup. The morphological development during the experiments was captured with a camera attached to the inside of the flume (C1) and a static camera at the outside of the flume (C2). Bed elevation was measured in still flow with an echosounder (E) along 10 transects (dashed lines). Flow velocities were measured separately with a Vectrino-II, which was installed at the channel centerline. (c) Ten transects were measured along the circumference of the flume, each 2.34 cm apart in transverse direction, starting at 4.5 cm from the walls of the flume.

lid and floor rotation at which the centrifugal force of the floor rotation balances the centrifugal force of the lid rotation, with the result that the secondary flow is minimalized and the flume can be used as an infinite straight river reach. Booij (1994) reports an optimal ratio of about 1.8, independent of the magnitude of the lid and floor rotation. Additionally, he measured a uniform streamwise shear stress across the width of the flume at this ratio. Here we employ the possibility to not only minimalize secondary flow, but also to control the secondary flow magnitude, without which no large transverse bed slope would develop.

Rotation of the flume floor also adds an outward-directed centrifugal force on the sediment, which effectively results in a rotation of the gravity vector. This can be expressed as a slope towards the outer bend related to this effective direction of gravity ($tan(\eta)$):

$$tan(\eta) = \frac{\omega_f^2 r}{g} \tag{8}$$

where ω_f = angular velocity of the flume floor (rad/s) and r = radius of the flume (m). However, with the current experimental settings this results in maximum slopes of 0.01 m/m, which is insignificant compared to the much steeper (up to 0.5 m/m) equilibrium transverse slopes in the morphodynamic experiments. Therefore, we will ignore the effect of centrifugal forces on the sediment in the remainder of this paper.

To determine near-bed streamwise and normal flow velocity without intrusive measurement techniques in flows with suspended sediment, analytical relations were derived as a function of the rotation rates of flume lid and floor. For verification and calibration, we ran 186 experiments for basic flow measurements in the center of the channel over flat bed conditions. More sophisticated numerical flow modeling representing details of this 3-D flow is outside the scope of this paper.

We conducted 224 morphodynamic experiments for several sediments ranging from fine sand to fine gravel, including low-density walnut grains, and the technically largest possible range of sediment mobilities and secondary flow intensities. We ran each experiment until morphological equilibrium, meaning that neither transverse slope nor bed form dimensions changed appreciably. With the resulting average transverse bed slope and the estimate of the near-bed normal and streamwise flow velocity, the slope factor B of each experiment could be determined (equation (2)). Slope factors of all experiments were then used to find a general relation between slope factor and sediment mobility for the entire experimental range (equations (3) and (4)), and compared to the values for α, α_c, and β found in literature for specific ranges of sediment mobility. Below we detail methods of flow measurement and modeling, sediment properties, experimental conditions, and measurement of morphology.

3.2. Measurement and Analytical Approximation of Flow Conditions in the Annular Flume

Flow velocities in streamwise and transverse direction were measured with a Vectrino-II, an acoustic Doppler velocity meter, at the center of the flume during 2 min. The Vectrino-II collects 16 data points in vertical direction in a range of 3 cm, with the most accurate measurement in the middle of this range. We chose to measure 0.5–3.5 cm above the bed, since in this range the highest normal flow velocities were recorded and furthermore, the objective is to study the effect of near-bed flow characteristics on sediment transport. Flow velocity measurements were done separately from the slope experiments and only on a flat bed, since it was not possible to measure near the bed when bed forms were present. In total, 186 flow velocity measurements were conducted under systematically varied angular velocities of both the lid and the floor, and above flat sediment beds without bedforms with median grainsizes of 0.26 and 1 mm. Angular velocities of the lid ranged from 0.16 to 0.90 rad/s, which corresponds with tangential velocities at the centerline between 0.30 and 1.67 m/s, and floor rotation was varied between 0 and −0.42 rad/s (0.78 m/s). Henceforth, lid and floor rotation will be expressed in tangential velocity at the centerline. The range in rotation velocity was restricted by the measurement range of the Vectrino-II, which gave large scatter at high angular velocities and when saltation or suspension concentration was too high. Measured flow velocities were reduced to a median streamwise and normal flow velocity, to be able to relate them to measured transverse slopes in the morphodynamic experiments. Vectrino-II data were then filtered by removing data points with a correlation less than 80%, taking the median of the time series per elevation and using the maximum value. This method of determining the average flow velocity produced significant scatter for unclear reasons, especially in normal flow velocities, and it was therefore not possible to fit a clear trend through the data to

extrapolate for higher angular velocities. Therefore, a simple analytical model was developed to predict streamwise and normal flow velocities at any combination of angular velocities.

Our analytical flow model is based on the assumption that shear stresses and centrifugal forces caused by lid and floor rotation, which drive the flow in the annular flume, are balanced by frictional forces of the lid and the walls of the flume. The trend in streamwise flow velocity is based on the model of Booij (1994), who found a reasonable agreement with flow velocity measurements in the same annular flume, but with a smooth bed without sediment. He assumed that shear stresses should cancel around the axis of rotation and therefore used the average value of the absolute tangential velocity (U) of the lid (l) and floor (f) at the center of the flume, multiplied with the ratio in surface area of the lid and flume. This ratio accounts for the larger surface area of the floor and sidewalls that apply shear to the water, and therefore have a larger influence on the average flow velocity than the lid. For the dimensions of the flume in this study, this ratio would be 0.78. However, in the current model this ratio is represented by a factor A_{s1} and is calibrated on measured data to account for unknown effects of three-dimensional flow patterns on the nonlinearity of the velocity profile. Furthermore, due to the sediment bed, in the current experiments the floor has a higher friction coefficient than during the measurements of Booij (1994), and therefore only a fraction of the floor velocity is transferred to the flow. This fraction is indicated with a second calibration parameter A_{s2}, which is absent in the model of Booij (1994). The resulting approximation for the streamwise flow velocity is:

$$u_s = A_{s1}\frac{U_l + A_{s2}|U_f|}{2} \tag{9}$$

The trend in normal flow velocity is determined using a model of a cross section of the flume. Here, it is assumed that the centrifugal force generated by the lid affects the top half of the water column, while floor rotation influences the bottom half. Since the pressure difference between the top half and the bottom half of the water column at the outer bend drives the secondary flow, the difference in lid and floor centrifugal acceleration is used as driving centrifugal force. This force is balanced by friction exerted along the lid, side walls, and sediment bed. The resulting approximation of the normal flow velocity is as follows:

$$u_n = \frac{A_{n1}HW(U_l - A_{n2}|U_f|)}{r(c_w(W+H)+c_bW)} \tag{10}$$

where H= water depth (m), W= width of the flume (m), and c = friction coefficient for the walls and lid (w), and the bed (b). A_{n1} and A_{n2} are calibration factors, accounting for nonlinearity of the velocity profile and the relatively larger influence of floor rotation on the average flow velocity due to a larger cross-sectional surface, respectively. The full derivation is given in Appendix A. When the ratio of lid to floor rotation is equal to A_{n2}, secondary flow is minimal and an infinite straight river section can be simulated. Booij (1994) stated this ratio is around 1.8 for the dimensions of the flume used in the current experiments.

Since only lid and floor tangential velocities are included in these equations as characteristic flow velocities for parts of the cross section, the magnitude of the resulting streamwise, and normal flow velocity are only a coarse approximation. Therefore, the measured flow velocities are used to calibrate the magnitude of the predicted flow velocities, while the trend of the analytical flow model is considered to correctly represent that of the measured flow velocities. We consider this the most parsimonious method as lid and floor tangential velocities and grainsize are the only variables.

3.3. Experimental Conditions and Data Collection

The annular flume used for the experiments described here has a radius of 1.85 m at the centerline and a rectangular cross-section with a width of 0.30 m and an adjustable height up to 0.47 m (Figure 2a). In our experiments, the lid is fixed at a height of 0.36 m above the flume floor. Each experiment started with a uniform horizontal sediment bed with a thickness of 0.15 m, resulting in an average water depth of 0.21 m. Lid rotation can be varied over a continuous range up to 3.7 m/s. For safety reasons, an angular floor velocity of 1.2 m/s was not exceeded.

Sediment size, floor rotation, and lid rotation were systematically varied in order to isolate the effect of a large range of near-bed flow conditions and sediment mobilities on the transverse slope, covering all sediment transport modes and bed state regimes. In Table 2 the range in sediment characteristics, sediment mobility, and secondary flow intensity is summarized, together with the number of experiments per

Table 2
Range in Sediment Characteristics, Sediment Mobility, and Secondary Flow Intensity of Each Sediment Type, Summing to a Total of 224 Experiments

P (kg/m^3)	D_{50} (mm)	D_{10} (mm)	D_{90} (mm)	nr runs	θ	$\tan\delta = \frac{u_n}{u_s}$
2,650	0.17	0.12	0.21	34	0.02–1.59	−0.24 to 0.19
2,650	0.26	0.19	0.33	23	0.03–1.16	−0.04 to 0.17
2,650	0.37	0.23	0.63	30	0.02–0.90	−0.11 to 0.16
2,650	1.0	0.85	1.16	45	0.02–0.41	−0.10 to 0.13
2,650	2.0	1.7	2.5	31	0.02–0.29	−0.03 to 0.11
2,650	4.0	3.15	5.6	37	0.04–0.19	−0.02 to 0.08
1,300	1.55	1.25	1.66	24	0.02–0.31	0.01–0.11

sediment type. Values for all experiments are given as supporting information. The parameter space covered by the experiments was designed and determined using the bed form stability diagram of Van den Berg and Van Gelder (1993), which plots sediment mobility against nondimensional grain sizes, and distinguishes bed state stability fields of no motion, ripples, dunes, and upper-stage plane bed (USPB). Grain sizes have been normalized as described by Van Rijn (1984a) to remove the effect of fluid viscosity and density. We assume that lower-stage plane bed occurs around the beginning of motion as observed in some bed slope experiments. We chose uniform sediments with median grainsizes of 0.17, 0.26, 0.37, 1.0, 2.0, and 4.0 mm and a density of 2650 kg/m^3, to ensure a transition from both hydraulic smooth to hydraulic rough conditions and across the ripple-dune threshold. Additionally, we used low-density granular walnut shell with a density of 1300 kg/m^3 and a median grainsize of 1.55 mm to test the effect of centrifugal forces generated by the flume floor. Henceforth we collectively name the sands $<$0.5 mm fine sand and the coarser sediments coarse sand and fine gravel.

Morphological development was registered using time-lapse photography and echosounding. Photographs were taken on both the inside and outside of the flume with a constant time interval, ranging from 5 to 300 s depending on the expected duration of the experiment. The camera on the outside was not attached to the flume and thus captured the development of the entire flume when floor rotation was added, while the camera at the inside was attached to the floor, consequently registering the development of a fixed segment (Figure 2b). The experiment was ended when the transverse bed slope and the bedforms were in equilibrium with the flow conditions. This took of the order of an hour for the high mobility experiments to a few days for the lowest mobility experiments. Experiments where dune troughs touched the solid flume floor were excluded. Afterward, the morphology was measured in still flow with an echosounder over 10 transects in streamwise direction, each 2.34 cm apart in transverse direction (Figure 2c). To allow filtering for sonic noise, the effective spacing of echosounder recordings was between the 1.2 and 1.4 mm in streamwise direction, depending on the circumference of the measured transect. The footprint of the echosounder is about 2 cm at average bed level.

Data were gradient-filtered for outliers and gridded for presentation, but the full data set was used for data reduction of resulting morphologies to one transverse slope value per experiment in the following steps. For each transect the median bed level over the entire flume length was determined. A linear trend was fitted by least-squares through eight of the ten data points across the flume to obtain the average transverse slope, excluding the two transects near the flume wall. Average transverse slopes of all experiments are reported in the online supplement. Additionally, the 16−84 and 5−95 percentiles of the bed levels along the transects were determined to represent spatial variation including bedforms along the flume. These values are used for analysis in combination with modeled flow velocity.

4. Results

In this section, we first evaluate the trend in flow velocity at specific ratios of lid and floor angular velocities, and then describe the trends in the spatially averaged transverse bed slopes. Finally, we seek relations between near-bed flow conditions, sediment mobility, and average equilibrium transverse bed slope.

4.1. Flow Velocity and Bed State at Specific Angular Velocities

The best fit of the analytical flow velocity model on the measured flow velocities was obtained with calibration parameters $A_{s1} = 0.65$ and $A_{s2} = 0.5$ for streamwise flow velocities, and $A_{n1} = 0.025$ and $A_{n2} = 2.5$ for normal flow velocities. Results show that streamwise velocities increase both with increasing lid rotation (Figure 3b) and with increasing counterrotation of the floor (Figure 3d), due to the larger difference between absolute lid and floor angular velocities. The linear relation of equation (9) shows a reasonable similarity with the data (Figure 3f) and an A_{s1} of 0.65 is similar to the 0.78 obtained by Booij (1994) and lower as expected because of higher bed friction.

Normal flow velocities increase when lid rotation is increased and can be described with a linear relation for a given floor rotation (Figure 3a). When lid rotation is constant and the counterrotation of the floor increases, normal flow velocities generally decrease as modeled (Figure 3c). Our data show that the ratio of lid to floor angular velocity for which the secondary flow intensity is minimal and reverses toward the outer wall is about 2.5 (A_{n2}), where Booij (1994) found a ratio around 1.8. Our ratio is higher due to the added roughness of the sediment bed. When floor rotation is increased even further, and this ratio therefore further decreases, the centrifugal force created by the floor rotation is dominant and as a result, secondary flow reverses and the normal flow velocity is directed toward the outer bend near the bed. However, when the flow velocity vector changes direction from the inner bend toward the outer bend the data deviate from the model, since the data shows a sharp transition in normal flow velocities. Furthermore, the data also deviates from the model for low counterrotation rates, where a local increase is observed before flow velocities decrease. As a result, the modeled linear trends look similar to the measured data except for the initial increase in velocity and the sharp transition when normal flow velocities change direction. Consequently, normal flow velocities are underpredicted for low ratios of lid to floor rotation where secondary flow reverses toward the outer bend, and overpredicted for low floor rotation, i.e., high ratios of lid to floor rotation (Figure 3e). This will be considered in later interpretations of bed slope data. Since negative normal flow velocities do not occur in natural river bends, the morphodynamic experiments with a flow velocity vector directed toward the outer bend will not be taken into account when determining the trend in transverse slope parameters.

The parameter space covered by the morphodynamic experiments contains a large range in secondary flow intensity (Figure 3) and sediment mobility for each grainsize, and therefore covers most bed form stability fields (Figure 4). Figure 5 shows examples of the typical bed form morphologies in the experiments. With fine sand we obtained bed states ranging from a lower-stage plane bed, across the ripple-dune threshold, to an upper-stage plane bed (USPB). In the experiments with coarse sand and fine gravel, including the experiments with low-density sediment, dunes developed and USPB was not reached. Observed beginning of sediment motion occurred at Shields numbers around the Shields curve for the beginning of sediment motion (Kleinhans et al., 2017; Soulsby et al., 1997). The transition from ripples to dunes in the fine sand experiments is characterized by dunes with superimposed ripples (e.g., Ashley, 1990; Ten Brinke et al., 1999; Venditti et al., 2005). The lines separating the ripple and dune fields therefore indicate a transition zone rather than a hard threshold (Kleinhans et al., 2017).

4.2. Equilibrium Morphologies

During the experiments a transverse slope developed toward either the inner wall or the outer wall. When flow conditions favored bedforms, they started to develop immediately at the start of each experiment (Figure 5). Dune height developed at the same rate as the transverse slope, but dune length needed more time to attain equilibrium because of dune splitting and merging processes. In the absence of dunes, on plane bed or with ripples, the transverse slope was fairly uniform along the flume. When dunes were present, the equilibrium transverse slope was largest in the dune trough but almost horizontal on the dune crest (Figure 5a). Furthermore, dune crests were aligned obliquely to the streamwise flow direction.

When sediment mobility was low, the transverse slope did not develop over the entire width. Since flow velocities are lower at the inner bend than at the outer bend, the inner part of the flume was still below the threshold of sediment motion. This effect was most clearly observed in the experiments with relatively coarse sediment, but was also present at the experiments with finer sediment. Thus, sediment mobility has a large effect on the average transverse slope near the threshold for motion. The effect of the glass walls of the flume on the morphology was limited to about 2 cm from the walls, while the outer bed level

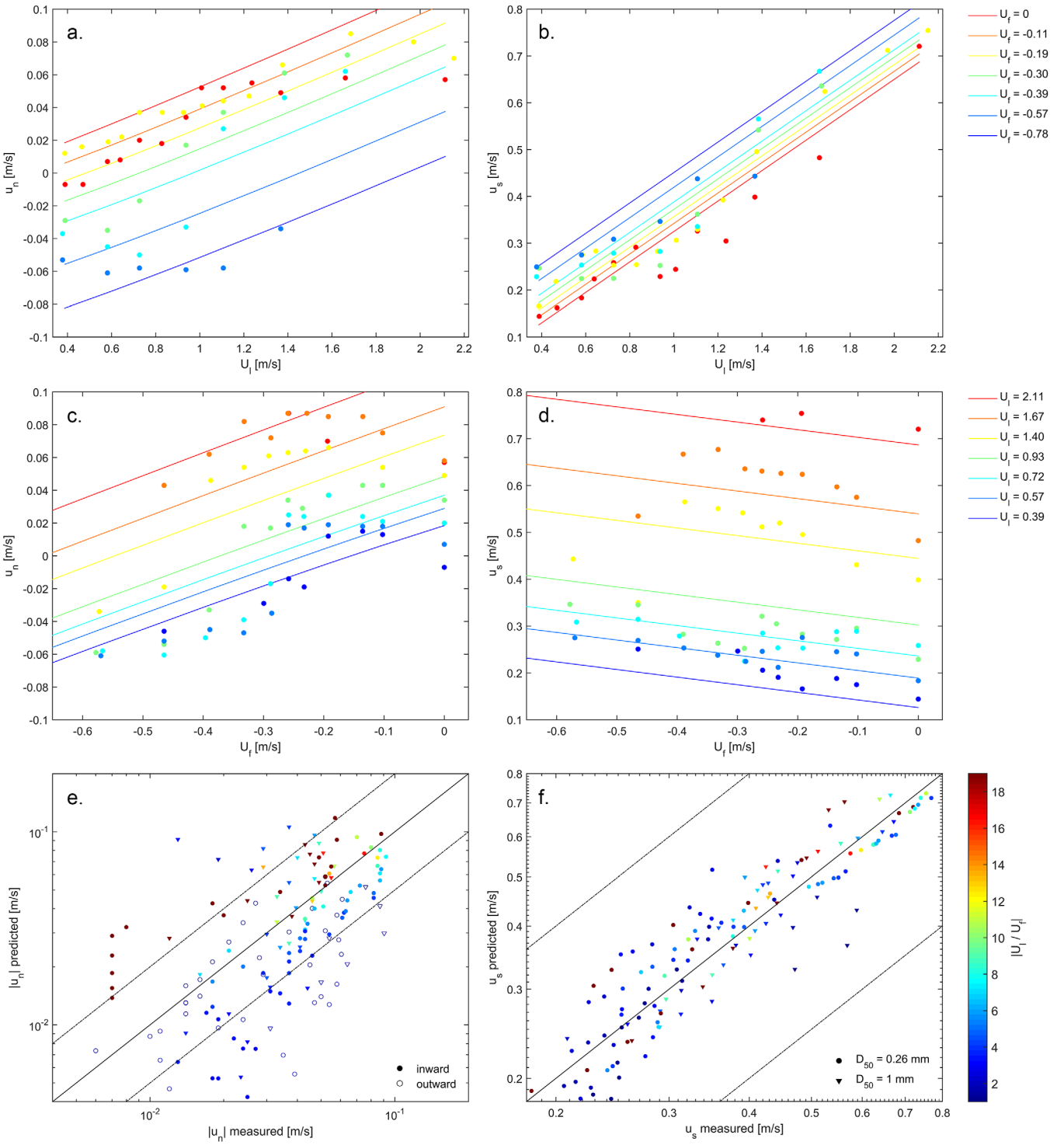

Figure 3. Measured (scatter) and predicted flow velocities (lines) for a range of lid and floor angular velocities used in the experiments. (a and b) Variation in normal and streamwise flow velocity with lid rotation, where separate lines and colors indicate a constant floor rotation. (c and d) Variation in normal and streamwise flow velocity with increasing counterrotation of the floor, where separate lines and colors indicate a constant lid rotation. (e) Predicted against measured normal flow velocities for a range in lid to floor rotation ratios (color scale). Flow is either directed toward the inner bend (positive values) or toward the outer bend (negative values). $R^2 = 0.78$. (f) Predicted against measured streamwise flow velocities, $R^2 = 0.90$. Dashed lines indicate deviation of a factor of 2.

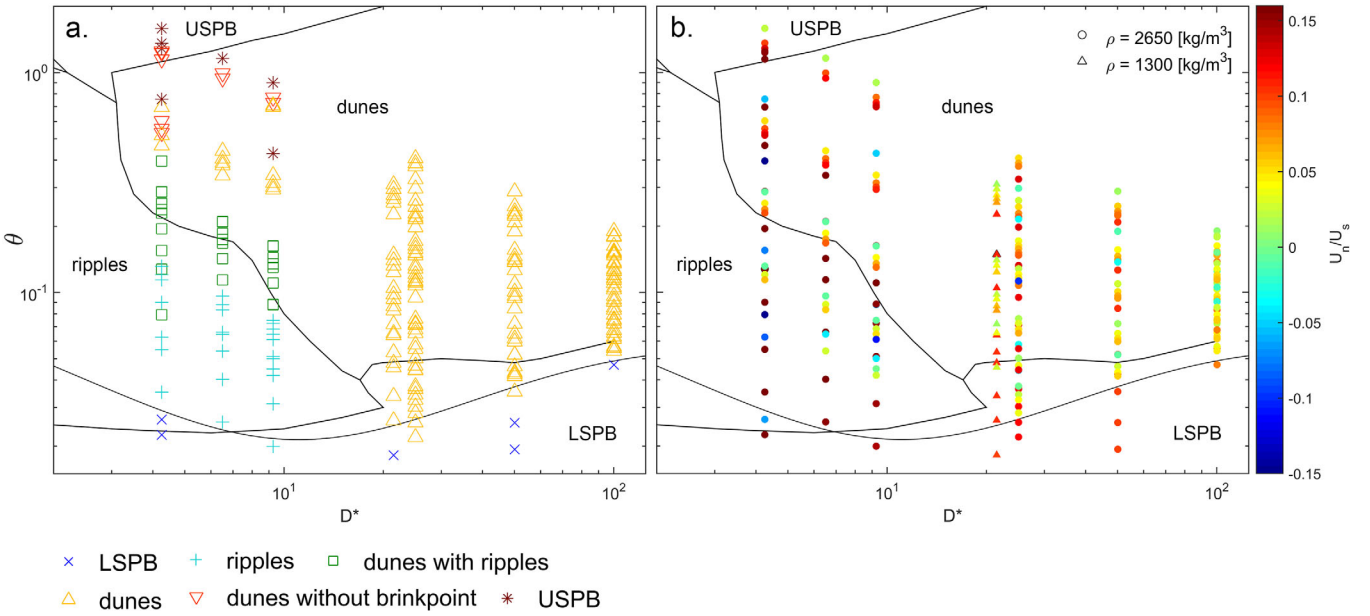

Figure 4. Parameter space covered by the experiments plotted in the bed form stability diagram of Van den Berg and Van Gelder (1993), with stability fields of lower-stage plane bed (LSPB), ripples, dunes, and upper-stage plane bed (USPB) indicated. The thick black line indicates the Shields curve for the beginning of sediment motion of Soulsby et al. (1997). (a) Observed bed states in the experiments (symbols). (b) Experimental range in secondary flow intensity (color scale) calculated from lid and floor rotation. For the experiments with coarse sand and fine gravel, sediment mobilities were limited by the maximum angular velocity of the lid.

measurements start at 4.5 cm from the wall. However, to make sure we did not include any wall effects, the two measurement transects near the walls were excluded from analyses.

Figure 6 illustrates the morphology of several experiments with different grain sizes, sediment mobilities, and secondary flow intensities, as well as the corresponding quantile bed levels in transverse direction. When lid rotation increased without floor rotation, the average transverse slope did not increase significantly from low to high mobility (Figures 6a and 6b). However, bedforms increased in height with increasing lid rotation and therefore the variation in bed levels increased.

On the other hand, when the inward-directed secondary flow decreased through increasing floor rotation whilst sediment mobility (θ) was kept constant, the average transverse slope depended strongly on secondary flow intensity (Figures 6c and 6d). When the secondary flow intensity became negative, and thus normal flow velocities near the bed were directed outward, a steep slope developed toward the outer wall of the flume. As observed in the flow direction data, this transition from a slope toward the inner bend to a slope toward the outer bend was rather sudden, so that gentle slopes toward the outer bend are uncommon in our data. In addition, bedforms also decreased in height with decreasing secondary flow intensity and increased again when secondary flow was directed towards the outer wall, even though average sediment mobility remained the same. Furthermore, the orientation of dunes crests varied with changing secondary flow intensity.

Figures 6e and 6f isolate the effect of changing mobility while keeping secondary flow intensity constant. The average transverse slope hardly changes with sediment mobility once the sediment is mobile over the entire flume width. However, bed level variation, i.e., the area between the 5 and 95 bed elevation percentiles, varied strongly with mobility in fine sediment, which is the result of bed state transitions. With increasing sediment mobility, bedforms developed from ripples to dunes with superimposed ripples, plane dunes, and low-angle dunes without brink points on the transition to USPB. As a result, the variation in bed levels increased when dunes developed and decreased again when sediment mobility increased towards USPB. In coarse sand on the other hand, variation in bed levels merely increased due to an increase in dune height. Dunes did not flatten as only intermediate sediment mobility was reached.

4.3. Effect of Isolated Parameters on Average Transverse Slope

The above examples suggest relations of sediment mobility and secondary flow intensity with average transverse slope. Here we combine transverse bed slope, modeled secondary flow intensity, and sediment

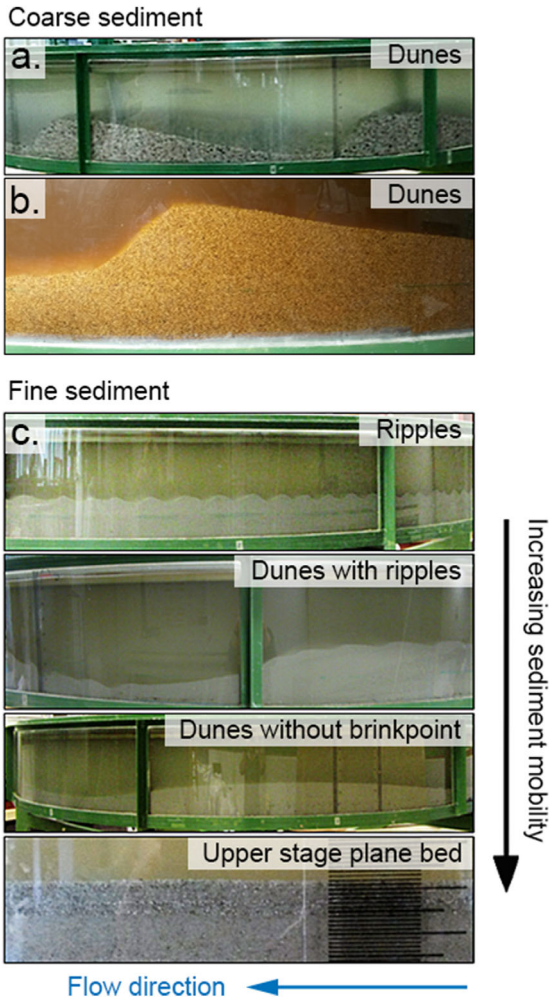

Figure 5. Examples of typical equilibrium bed states. (a) Dunes developed during experiments with coarse sand and fine gravel, (b) and with low-density sediment. (c) With fine sands the entire range of bed states from lower-stage plane bed, across the ripple-dune threshold, to upper-stage plane bed were obtained with increasing sediment mobility.

mobility of all experiments to explore the trends, and calculate slope factor B (equation (2)) for the experiments with secondary flow directed toward the inner bend.

Sediment mobility varied from just above the threshold of sediment motion up to 1.59 for the finest sand (Figure 7a). Despite this large range, no clear trend in average slope against sediment mobility is discernable, as a large variation in transverse slopes occurs at various ranges of sediment mobility. However, when sediment mobility approaches the beginning of motion, transverse slopes reduce. At the other extreme end of the possible slope range, transverse slopes never increased above 0.5 m/m, or about 29°, which is about the angle of repose of loose granular sediment.

On the other hand, transverse slope against secondary flow intensity shows a clearer trend. Slopes increase with secondary flow intensity, i.e., when the normal flow velocity component increases relative to the streamwise velocity (Figure 7b). However, there is still considerable scatter. The data, color-coded with sediment mobility in Figure 7b, suggest relatively lower increase in bed slope with secondary flow intensity with increasing sediment mobility. Furthermore, the restriction on transverse slope at relatively low sediment mobility is visible by the average slopes just above zero regardless of the secondary flow intensity. This shows there is no simple similarity collapse for transverse bed slope as a function of secondary flow and sediment mobility.

For the experiments with fine sand, the bed slope factor B increases monotonously with increasing relative sediment mobility up to a relative sediment mobility of about 6 (Figure 8a). This means that, given a constant secondary flow intensity, transverse slopes steepen with sediment mobility. For relative sediment mobilities higher than 6, the slope factor reaches a constant value for a given secondary flow intensity, suggesting independence of sediment mobility. For the coarse sediments, the slope factor first increases rapidly with increasing sediment mobility, but then abruptly decreases (Figure 8b). This local maximum is more pronounced for lower secondary flow intensities and coarser sediment. Above a relative sediment mobility of about 4, the slope factor appears independent of sediment mobility. However, for relatively low secondary flow intensities, the slope factor of a few experiments continues to decrease at relatively high sediment mobility.

The different trends of fine and coarse sediments and the existence of a local maximum bed slope factor B at intermediate sediment mobility suggests a relation with bed state. Various bed states were observed which appeared to influence the average transverse slope significantly, especially when dunes were present (Figure 5a). For experiments with almost equal secondary flow intensities, transverse slope increased with mobility when ripples are present, but upon dunes initiation the transverse slope hardly increased (Figure 8a). However, similar trends were observed for experiments with coarse sediment and only dunes (Figure 8b). Here, the local maximum in slope factor seems to coincide with low dune height to length ratio (Figure 8d), as well as the transition from rolling sediment transport to saltation (Figure 8c). We attempted normalization by a number of bed form dimensions and bed form-related friction parameterizations but none resulted in a similarity collapse of the data of fine and coarse sediment.

Experiments with low-density sediment followed the same trend in bed slope factor B with changing relative sediment mobility, indicating that sediment density has no first-order effect on equilibrium slopes. This is confirmed by the observation that the magnitude of the slope factor of the low-density experiments corresponds best with the experiments with a median grainsize of 2 mm (Figure 9b), rather than the

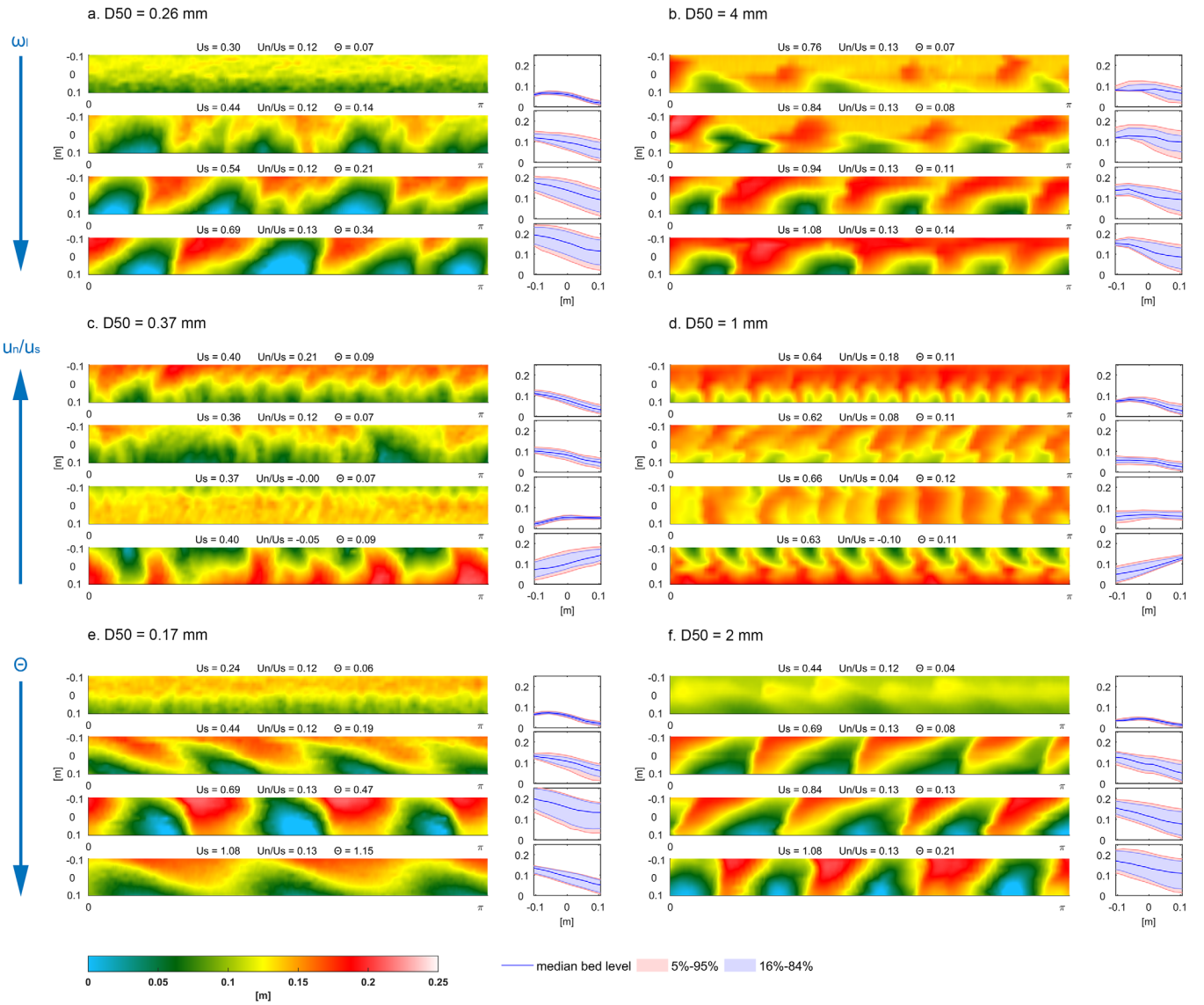

Figure 6. Example maps of bed elevation above the flume floor (color scale) on streamwise and normal coordinates, and data reduction to bed elevation percentiles across the flume. Flow is to the left; the inner bend is toward negative normal coordinates and only a semicircle of the bed is shown. Experiments are grouped to illustrate trends with grainsizes, lid rotation, secondary flow intensity, or sediment mobility with other factors kept constant. The average transverse bed slopes used in the remainder of this paper were calculated by linear regression on the median bed levels across the flume, excluding the outermost transects. Experiments where dune troughs touched the solid flume floor were excluded. (left plots) Fine sediments and (right plots) Coarse sediments with similar behaviors. (a and b) Experiments with increasing lid rotation with static floor. (c and d) Experiments with decreasing secondary flow intensity, while sediment mobility remains constant. (e and f) Experiments with increasing sediment mobility and constant secondary flow intensity.

experiments with a median grainsize of 1 mm (Figure 9a) which have corresponding nondimensional grain sizes (Figure 4), since grain sizes are normalized with relative density (Van Rijn, 1984a).

5. Discussion

We first discuss the relation between the transverse bed slope and the secondary flow intensity and the sediment mobility (expressed as Shields number) observed in the experiments, and then compare the observed trends with predictors found in literature and comment on the implications for morphodynamic modeling.

5.1. Influence of Secondary Flow Intensity and Sediment Mobility on Transverse Slope

Average transverse bed slope shows a relation with secondary flow intensity and proportionality factor *B*, as equation (2) by Van Bendegom (1947) suggests. However, there are two slope-limiting conditions not

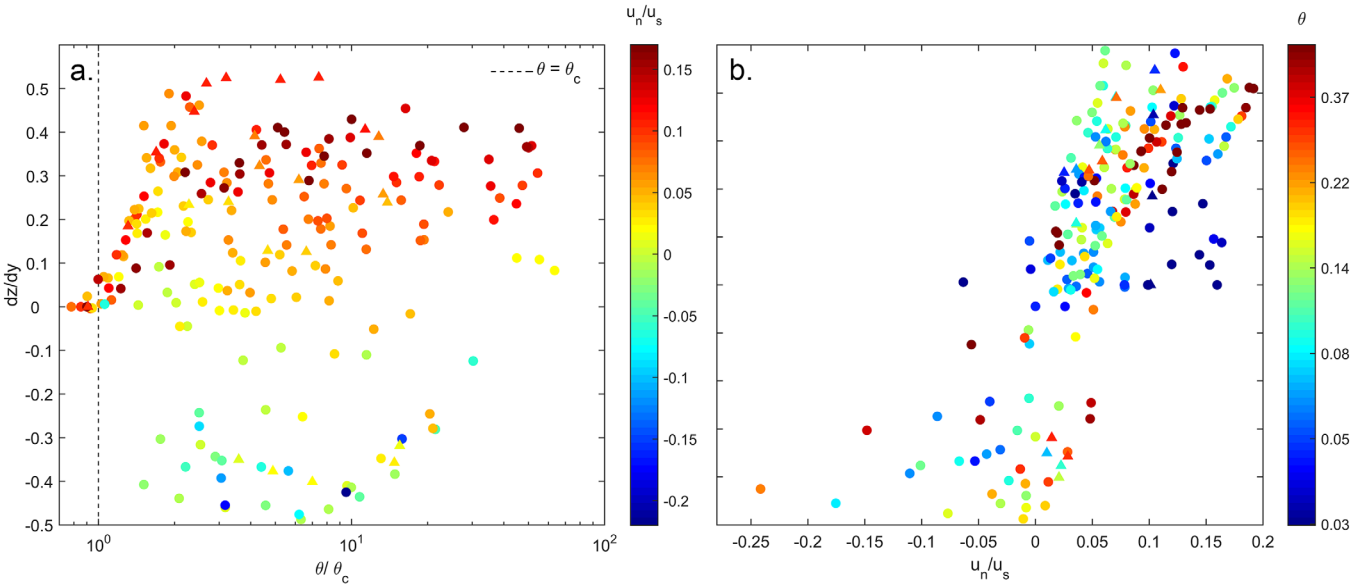

Figure 7. Average transverse bed slopes of all experiments. (a) Transverse slope against relative sediment mobility. Color scale indicates secondary flow intensity and direction. (b) Transverse slope against secondary flow intensity. Color scale indicates sediment mobility.

included in this relation. The first limit is the maximum angle that can be reached under the influence of gravity. Here this is slightly lower than the typical value for the angle of repose due to dilatancy of the sediment during transport (Kleinhans et al., 2011). The morphology was measured in still flow, while during the experiments this maximum slope could have been higher under stronger secondary flows driving the sediment upward. Second, the transverse slope cannot fully develop when width-averaged sediment mobility is close to the threshold of sediment motion and below it in the inner bend. Hence, the cross-sectionally averaged transverse slope remains low when sediment mobility is low, regardless of secondary flow intensity (Figure 7).

The limiting role of sediment mobility is also visible in Figure 8. Below a relative sediment mobility of 6, the slope factor B of fine sands depends on relative sediment mobility. For coarse sand and fine gravel, this dependence is visible up to a relative sediment mobility of 3. The proportionality factor B is lower than unity at small sediment mobilities, with lowest values of around 0.2 for fine sediments and 0.1 for coarse sediments, and rapidly increases above 1 for larger sediment mobilities. For coarse sediments, this increase in slope factor is even more pronounced, especially for experiments with relatively weak secondary flow and low transverse bed slopes. The nonlinearity of the relation between sediment mobility and slope factor suggests other processes covarying with sediment mobility also affect the proportionality of transverse slope to secondary flow intensity. We found that including the critical Shields number led to a better similarity collapse of trends in average slope of experiments with different grainsizes under the same conditions, which makes sense as the different sediments have different critical Shields numbers and therefore a different offset (Figure 10).

Furthermore, Figure 8 shows that the magnitude of the slope factor varies with different secondary flow intensities, suggesting the transverse slope is not linearly related to the secondary flow intensity with constant sediment mobility (equation (2)). However, low secondary flow intensities were underpredicted by the analytical flow model (Figure 3), so it remains unclear whether this trend is significant.

5.2. Influence of Bedforms and Sediment Transport Mode

The scatter in the data described above suggests that other processes are important. Here we discuss four processes: sediment transport mode, modified turbulence over the ripple-dune transition, the net effect of avalanching at dune slip faces migrating on a transverse bed slope, and flow steering in the troughs of oblique dunes.

First, the dominant mode of sediment transport changed with increasing sediment mobility (Bennett et al., 1998; Bridge & Bennett, 1992). The transition from rolling bed load toward saltating particles coincides with

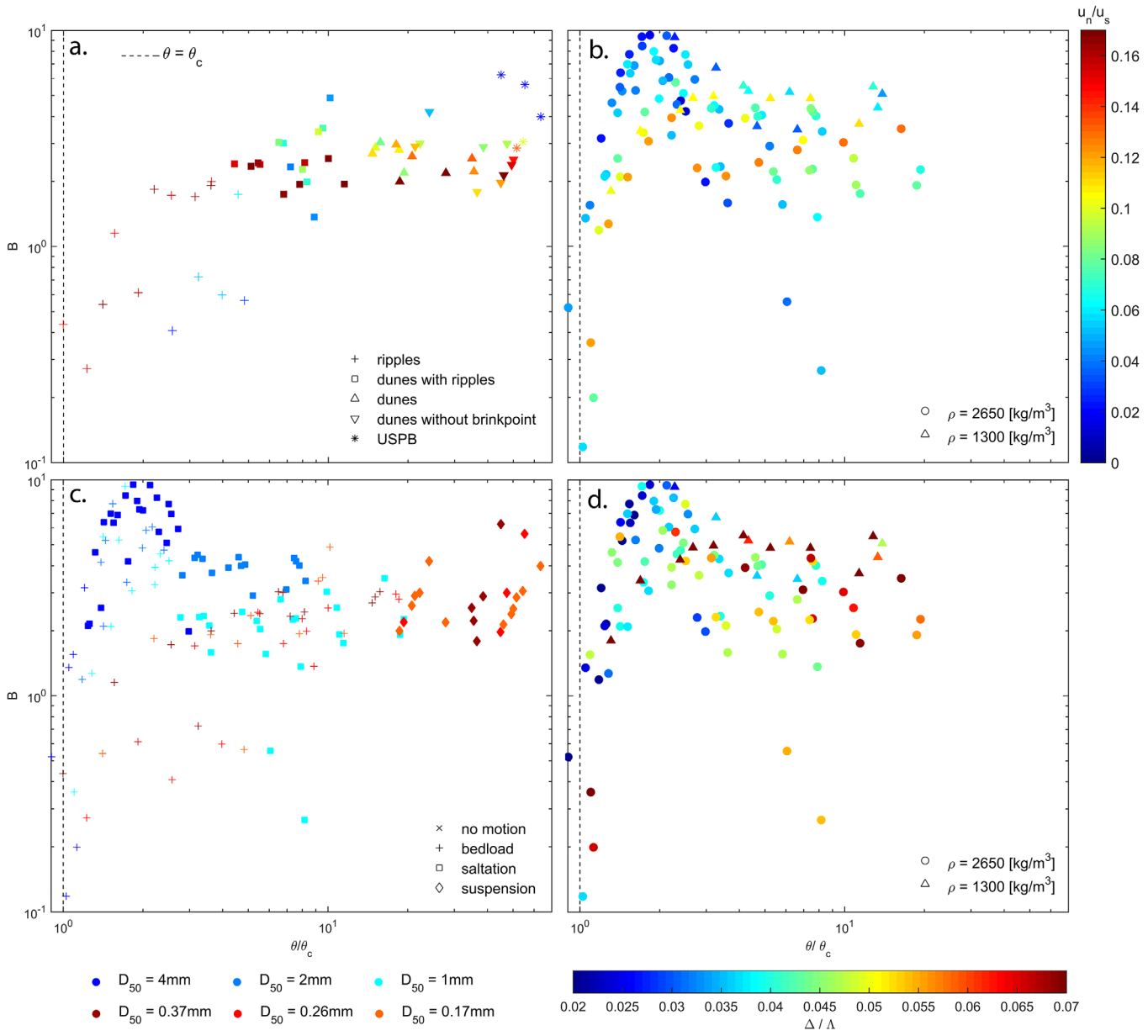

Figure 8. Trends in slope factor (equation (4)) against relative sediment mobility of all experiments with transverse slopes toward the inner bend. (a) Slope factor of the experiments with fine sands. Color bar indicates secondary flow intensity. (b) Slope factor of the experiments with coarse sands and fine gravel, including the low-density sediment. Color bar indicates secondary flow intensity. (c) Observed sediment transport mode of all experiments. Color indicates grainsize. (d) Dune dimensions of the experiments with coarse sand and fine gravel. Color bar indicates dune height to length ratio (Δ/Λ).

the local maximum in transverse slope observed during the experiments with coarse sand and fine gravel (Figure 8c). For fine sands, there is no local maximum, but instead the slope factor gradually increases with increasing mobility until suspension of sediment is present. Here, the slope factor is constant, which means that in this range transverse slopes are independent of sediment mobility and increase linearly with increasing secondary flow intensity (Figure 8a). However, this transition to a constant slope factor is not clearly related to the transition from dominant bed load transport to suspended transport and therefore it remains unclear if this is a causal relation.

Second, bed forms were prominent in many experiments. When the bed state of the fine sand experiments transitions from ripples to dunes at higher sediment mobilities, the increase in average slopes decreases and as a result the slope factor reaches a constant value (Figure 8a). Compared to the ripple regime, this

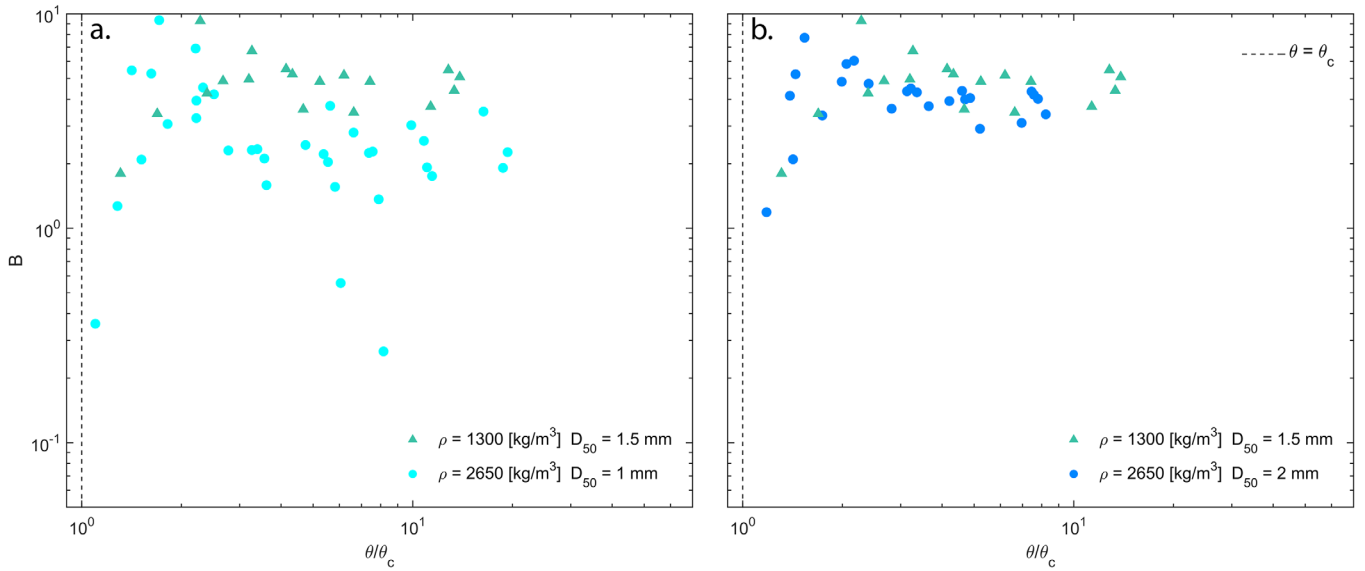

Figure 9. Trend in slope factor (B) against relative sediment mobility for experiments with low-density sediment, compared with experiments with normal sediment with median grain sizes of (a) 1 mm and (b) 2 mm.

means a relative increase in downslope sediment transport with increasing sediment mobility that linearly depends on dune height. Sieben and Talmon (2011) found that the increase in downslope sediment transport on lee sides of dunes resulted in lower transverse slopes, which is caused by the fact that avalanching on the dune slip face is in downward direction rather than perpendicular to the bed or in the direction of dune migration. In our experiments, long dunes, and thus fewer dunes, were observed at intermediate sediment mobilities, where also the maximum slope factor was observed during experiments with coarse sediments (Figure 8d).

Third, in the case of fine sands, the independence of sediment mobility when dunes are present could be explained by a change in turbulence as ripples transition to dunes (e.g., Bennett et al., 1998), which would affect flow through the friction, and sediment transport through the near-bed turbulence. This agrees with the observations of Wiesemann et al. (2006), who found that transverse bed slopes become independent of sediment mobility when dunes start to develop, although they observed a decrease in downslope sediment transport. However, our comprehensive data set shows a similar independence of transverse slope on higher sediment mobility for coarse sediment where ripples cannot form, so the ripple-dune transition in itself cannot be the explanation.

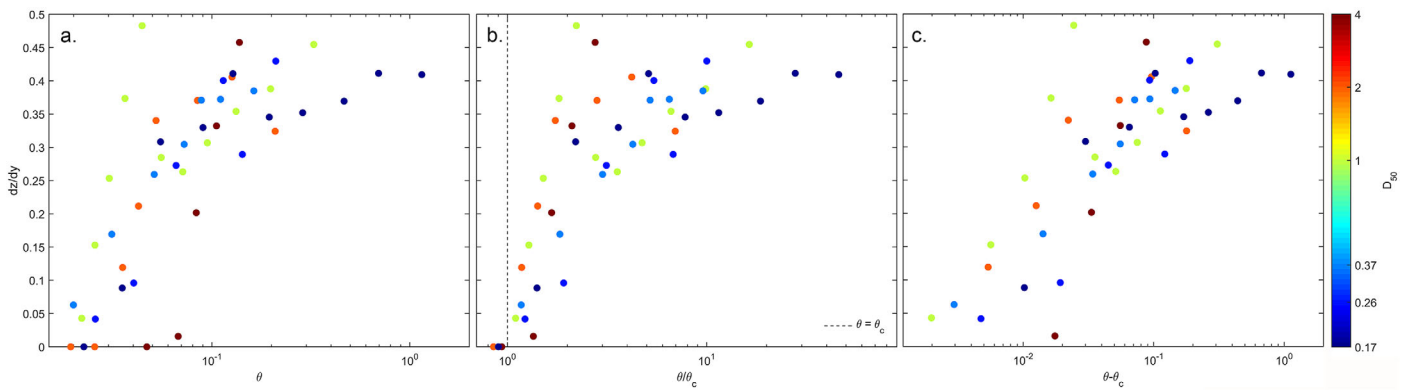

Figure 10. Average transverse bed slopes of experiments with only lid-rotation against (a) absolute sediment mobility, (b) relative sediment mobility, and (c) excess sediment mobility for all grain sizes (color scale). The best similarity collapse is attained for relative sediment mobility.

Fourth, Dietrich and Smith (1984) and Kisling-Moller (1993) qualitatively observed that the near-bed transverse flow is affected by the presence of oblique dunes in curved flow. In the annular flume, slope was largest in the dune trough and almost horizontal on the dune crest, so that the maximum slope in the dune trough was about 2 times larger than the average slope. These large variations in transverse slopes along the flume show that average values for flow velocities and slopes are not necessarily representative, and possibly cause unexplained scatter in our trends. Dunes must have had a substantial influence on flow patterns because of their large height relative to water depth. As a result, transverse flow may have lined up with, and concentrated in the troughs of oblique dunes. Indeed, differences in the obliquity of dune crests were observed between experiments, which could have been an effect of secondary flow and this flow concentration, or the cause of enhanced secondary flow. Alternatively, the obliquity was the result of the secondary flow affected by bedforms. The above discussion shows a potentially large influence of dunes on secondary flow patterns. Also, the transverse bed slope strongly depended on the position on the dunes. Future analysis of flow velocity patterns over large dunes is needed to unravel which of the above hypotheses really matter for the transverse bed slopes in the experiments, and how such trends hold for full-scale natural systems with lower dunes relative to water depth.

5.3. Comparison With Existing Bed Slope Predictors

Published predictors were derived for one sediment transport mode or bed state to study its separate effect on the transverse bed slope effect, and were calibrated and verified with experiments within a specific range in flow conditions and sediment mobility to isolate this mode or bed state. The predictors are therefore only valid for the parameter space of these experimental conditions, which are indicated in Table 1. For example, the predictor of Ikeda (1984) that is used in Delft3D is only valid for median grain sizes around 0.15 mm and a sediment mobility between 0.10 and 0.23. All predictors include slope factors which are based on a linear relation with slope, i.e., a constant α or α_c, and a power function of sediment mobility, which means that friction parameters and calibration parameters are constant. However, our objective is to obtain parameters that cover all sediment transport modes and bed states, so that this relation can be used in large-scale and long-term modeling where all processes act in concert. The current results show a nonlinear relation for the slope factor when plotted as a function of relative sediment mobility (Figure 8) as they cover the limiting effect of low sediment mobility, the effect of the angle of repose and effects of different bed states and sediment transport mode due to experiments with grain sizes varying between 0.17 and 4 mm and sediment mobility between 0.018 and 1.59. Consequently, the trend of the slope factor with sediment mobility from this study is more complex than that of the existing predictors, with an α or α_c and β that are not constant. Based on current results, the slope factor should thus be described with a different function than equation (4) to adequately describe the nonlinear dependence on sediment mobility. However, to be able to compare the slope parameters of existing predictors to the experimental results, a preliminary fit of the slope factor over relative sediment mobility is plotted in Figure 11 with constant values for α_c and β per median grainsize:

$$B = 25 D_{50}^{0.37} \left(\frac{\theta - \theta_c}{\theta_c} \right)^{0.2} \tag{11}$$

In view of our understanding of the sediment transport process reflected in transport predictors, it is necessary to include a critical shear stress, especially when different sediment sizes are considered. Additionally, it is necessary to start at a relative sediment mobility of 0, to start with a flat bed at the beginning of motion. Consequently, the resulting formulation of relative sediment mobility is the same as the mobility parameter in the sediment transport predictor of Van Rijn (1984a). Furthermore, the fit is grainsize-dependent due to significant differences in the magnitude of the slope factor. To further account for the difference between fine sediment and coarse sediment, a different function is plotted for experiments with coarse sediment and a relative sediment mobility lower than 2.5:

$$B = 50 D_{50}^{0.37} \left(\frac{\theta - \theta_c}{\theta_c} \right) \tag{12}$$

which empirically covers the abrupt transition observed in the data but is as yet unsatisfactory for modeling purposes where sudden transitions and thresholds may cause instability.

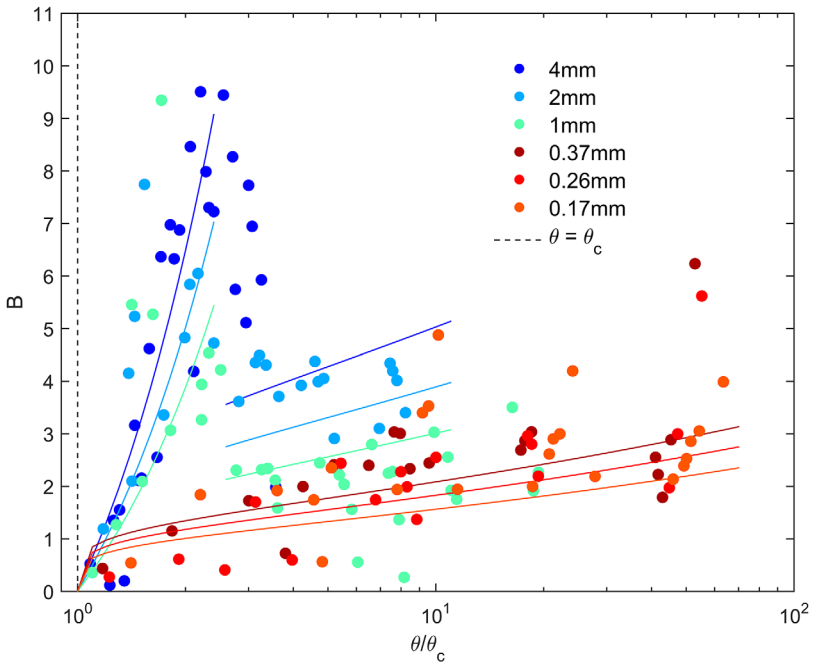

Figure 11. Empirical fits to experimentally determined slope factors as a function of relative sediment mobility and grain-size. The fitted functions have a similar shape as existing relations found in literature (equations (11) and (12)).

This fit indicates α_c varies between 1 (0.17 mm) and 1.34 (0.37 mm) for fine sand, and between 1.94 (1 mm) and 3.24 (4 mm) for coarse sand and fine gravel with relatively higher sediment mobility. However, this fit does not describe the independence from sediment mobility of the slope factor, which is reached at a lower sediment mobility for coarse sands and fine gravel than for fine sands. For a relative sediment mobility lower than 2.5 and coarse sediment, α_c varies between 3.9 (1 mm) and 6.5 (4 mm) and β is equal to 1, representing the sharp increase in slope factor at low sediment mobility. Compared to literature the predictors based on a power function of Shields number all underestimate the slope factor significantly and thus overestimate the downslope sediment transport and therefore lead to flatter slopes than we observed (Figure 12c). Predictors that include a critical sediment mobility more adequately describe the amount of downslope sediment transport for fine sands, but still overestimate slope effects for coarse sand and fine gravel (Figure 12c). The predictors of Engelund (1974) and Engelund (1975) are independent of sediment mobility and therefore cannot be valid for low Shields numbers. The value of 0.2 for β is lower than in literature, resulting in a lower increase in slope factor with increasing sediment mobility.

We can now examine the trends in our data in view of the assumptions behind the process-specific predictors (Table 1). First, in literature several predictors are specified for low sediment mobility and a plain bed configuration, with either bed load transport (Engelund, 1975; Hasegawa, 1981) or saltation (Francalanci et al., 2009; Parker et al., 2003; Sekine & Parker, 1992). In the current experiments, no plain bed was observed above the threshold of sediment motion, but we can compare these predictors with the trend in our data for experiments with bedload transport and saltation below a sediment mobility of 0.2, which is the maximum sediment mobility for which the predictor of Sekine and Parker (1992) is validated. Hasegawa (1981) defined a predictor based on both dynamic and static friction for bedload transport of fine sediment, with an α_c that is comparable to our fine sediment data in this range (Figure 12d). Parker et al. (2003) defined a predictor for coarse sediment based on a ratio between the critical sediment mobility for the cessation of sediment transport and for the beginning of motion, which is generally below unity and results in a slope factor that is comparable to our coarse sediment data around the transition to saltation. Therefore, we can conclude that for low sediment mobility the influence of transverse slopes on the beginning and cessation of motion mainly determines the equilibrium slope. However, the strong observed increase in slope factor with increasing sediment mobility for coarse sediment is not explained by existing predictors for low sediment mobility.

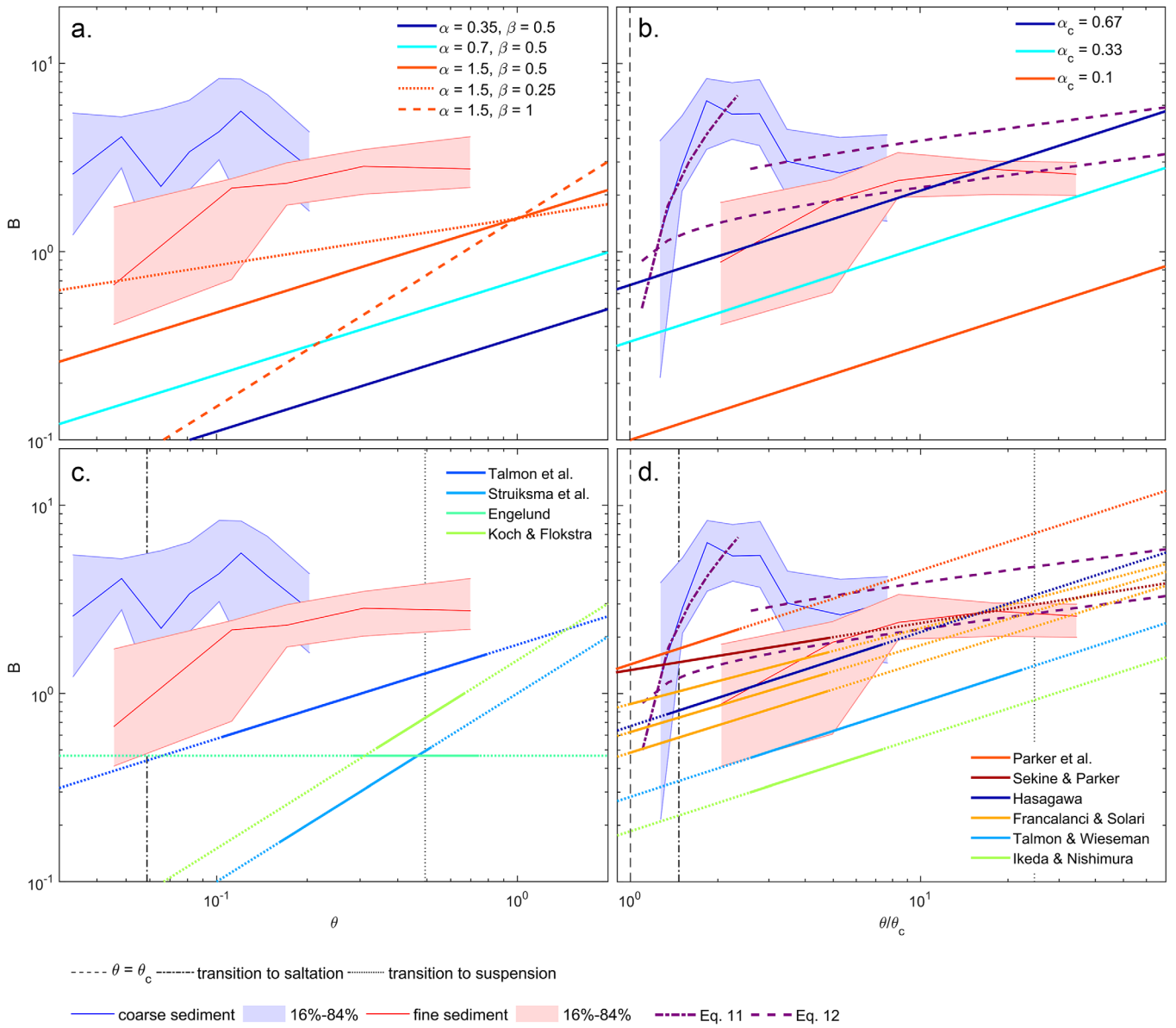

Figure 12. Comparisons of experimentally determined slope factors and predictors found in literature for sediment mobility ranging between the beginning of sediment motion and upper-stage plane bed. The experimental data are reduced to slope factor percentiles for small intervals of (relative) sediment mobility, split in two grainsize classes with distinct behaviors. The fitted functions based on the experimental data (equations (11) and (12)) are also shown. (a and b) Experimental data compared with generic predictors (equations (3) and (4)) with typical parameter values as used in morphological modeling based on either (a) sediment mobility or (b) relative sediment mobility. (c and d) Experimental data compared with specific existing predictors (Table 1), based on either (c) sediment mobility or (d) relative sediment mobility. The condition range for which an existing predictor is valid is indicated with a solid line, while outside this range the predictor is plotted with a dotted line. The nonlinear predictor of Francalanci and Solari (2008) is plotted for transverse slopes of (upper line) 0.3, (middle line) 12, and (lowest line) 25 degrees. Theoretical transition zones to saltation as defined by Bridge and Bennett (1992) and to suspension as defined by Van Rijn (1984c) are also indicated by vertical-dashed lines.

The predictor of Sekine and Parker (1992) assumes that saltating particles are less influenced by gravity than rolling and sliding particles because they have less frequent contact with the bed, with the result that the slope effect is less dependent on sediment mobility. Consequently, due to a β of 0.25, this predictor most accurately describes the trend in the current data for relative sediment mobilities higher than 4, for both fine sand and coarse sand and fine gravel. In this range, all coarse sand and fine gravel experiments showed saltation for which the predictor of Sekine and Parker (1992) was developed (Figure 8). At lower sediment mobilities, sediment mobility has a larger influence on slope effects, as described above, and here the predictor deviates from the data.

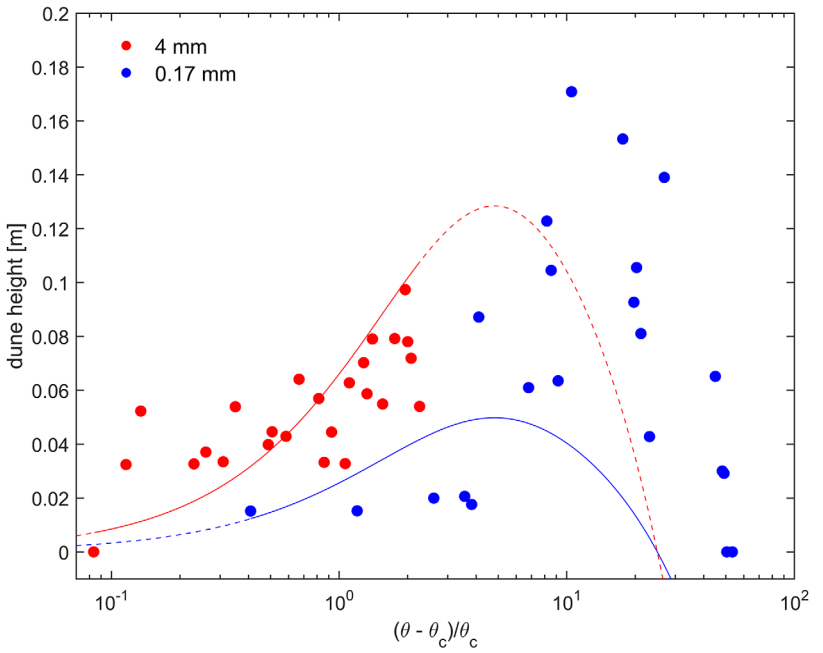

Figure 13. Comparison between the dune height observed in the experiments with a median grain size of 4 and 0.17 mm (scatter) and the dune height as predicted by Van Rijn (1984b) (lines). Solid lines represent the predictor for relative sediment mobility in the range of the experiments, while dashed lines show the whole trend of the dune height predictor from lower stage plane bed to upper stage plane bed.

Ikeda (1984) and Ikeda and Nishimura (1986) have a similar predictor, based on the balance between friction and drag force. The only difference between these two predictors is the addition of a sheltering coefficient by Ikeda and Nishimura (1986) that improves the fit with their experimental data. The resulting difference in α_c can thus be explained by the difference in experimental settings which were used to validate the theoretical model. Namely, the model of Ikeda and Nishimura (1986) is validated with conditions that favored ripples, while during the experiments of Ikeda (1984) dunes formed. Although these predictors deviate significantly from our slope parameters, this confirms that bed state can have a significant effect on the slope factor, as is observed in the current experimental data set and described in the previous section.

The difference in slope factor due to bedforms is also observed in the study of Talmon et al. (1995) and the empirical study of Talmon and Wiesemann (2006) who added a specific bed form calibration parameter to account for this. Talmon et al. (1995) showed that the difference between slope factors in natural rivers are in the order of two lower than slope factors in experiments with dunes, due to the relatively high bedforms compared to the water depth. Therefore, they used a slope factor based on the bed form height predictor of Van Rijn (1984b) to account for the increased bed friction. Van Rijn (1984b) predicts bed form height to depend on relative sediment mobility and a ratio between median grain size and water depth: $\left(\frac{D_{50}}{H}\right)^{0.3}$. Interestingly, our trend in slope factor also depends on a median grain size to the power of about 0.4 (equations (11) and (12)). In Figure 13, dune height as observed in the experiments with a median grain size of 4 and 17 mm is compared with dune height as predicted by Van Rijn (1984b). The predicted dune height for coarse sediment agrees with the observed dune height. The magnitude of the predicted dune height for fine sediment does not correspond with the data, but the increase in dune height with increasing relative sediment mobility is visible, as is the maximum around a relative mobility of 10 and the decrease when dunes are flattened toward an upper stage plane bed. This, together with the conclusion that bed state has a significant influence on the slope factor, confirms the use of an α_c that depends on the median grainsize to account for bed form friction.

5.4. Implications for Morphodynamic Modeling

Pending a more complete process explanation and better transverse bed slope relation, we here briefly interpret what the implications of our findings are for large-scale morphology and for morphodynamic

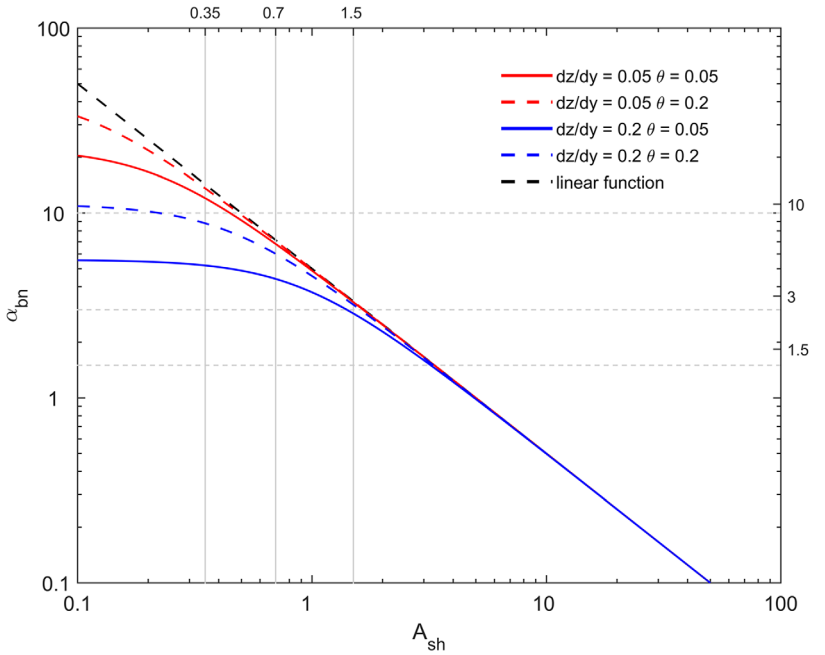

Figure 14. Relation between α_{bn} and A_{sh}, the input parameters of the two main options to calculate sediment transport on transverse bed slopes in the morphodynamic model Delft3D (equation (B1)). Colored lines indicate different combinations of transverse slope and sediment mobility, with a critical sediment mobility of 0.04. Gray lines indicate frequently used input parameters as described in section 2 and used in Figure 12.

modeling. At lower sediment mobility, slope effects are relatively high, resulting in smoother morphologies than expected from existing relations, while at environments with larger sediment mobilities slope effects have less influence, which is reflected in a higher slope factor and will result in steeper transverse slopes in otherwise the same conditions and in the absence of processes not studied here, such as lateral diffusion of suspended sediment. For coarse sediments, slope effects are the smallest at intermediate sediment mobility and here slopes are even steeper than at high sediment mobility under the same secondary flow conditions. This will result in for example a higher braiding index than expected from existing relations. Furthermore, current results suggest a change in sediment mobility has a larger effect at lower mobilities, compared with relatively high mobilities were the slope factor is almost constant with increasing sediment mobility. This effect is therefore especially important in areas with low sediment mobility where a significant difference in sediment mobility over time or space occurs, e.g., near channel banks and shoal margins. How exactly a nonlinear bed slope relation changes this local morphology remains to be studied by modeling.

The objective of this study was to obtain a general relation that is valid for all systems where various sediment transport processes and bed states can occur together, instead of the process-specific predictors subject to model operator choice. This relation is therefore more suitable for application in a morphodynamic model like Delft3D that is used across a wide range of environments and conditions in science and in engineering practice. As long as current morphodynamic models do not include a transverse slope relation that describes the nonlinearity with sediment mobility and the dependence on grain size as found in our data set, it is therefore tentatively advised to adjust input parameters α_c and β to the system that is modeled. This is a simplification in that changes in mobility away from channels and up bars are ignored. Equations (11) and (12) can be used as guidelines when determining these input parameters. In general, for systems with low sediment mobilities and grain sizes larger than 0.8 mm, where only dunes are expected to occur, β should be 1 and α_c around 5. For systems with higher sediment mobilities, a β of 0.2 and an α_c around 2.5 is advised. For fine sediments and all systems, α_c is lower, around 1. A calibration range of a factor 2 is acceptable to account for the uncertainty of the influence of relatively high bedforms in flume experiments. Appendix B describes the input parameters for Delft3D in more

detail, and a guideline to switch between the two methods for sediment transport deflection on transverse slopes.

Surprisingly, the magnitude of experimentally determined slope factors is similar or higher than slope factors in predictors used in Delft3D, which also means the parameter α_c is higher than the default value of 0.67 for most sediment mobilities and only lower than 0.33 near the beginning of motion (Figure 12b). Likewise, the α is always higher than a value of 1.5 (Figure 12a). This is at odds with the need to increase the slope effects by decreasing α or α_c in model calibration on measured bathymetry (e.g., Van der Wegen & Roelvink, 2012). Under all assumptions made in our work, this leads to the conclusion that the tendency of models to overdeepen channels is not a direct result of the shortcomings of current transverse bed slope predictors. Rather, it suggests that such calibration is necessary to compensate for other, hitherto unidentified model weaknesses such as issues with numerical schemes or missing processes.

Past work hints at a combination of processes and parameters that affect bed slopes indirectly (e.g., Kleinhans et al., 2008). First, the prediction of flow resistance can be improved, including the effect of bedforms. In Delft3D, a constant Nikuradse roughness coefficient results in steeper gradients between river banks and channels, while a uniform Chezy roughness implies a changing Nikuradse roughness coefficient with water depth and results in shallower channels and smoother morphology in general (Schuurman et al., 2013). Second, sediment transport predictors have different degrees of nonlinearity due to different power functions and different choices of including the threshold for motion. Third, the choice in sediment transport predictor determines if suspended sediment is taken into account. Van der Wegen and Roelvink (2012) decreased the α_c by an order of magnitude for the Van Rijn sediment transport predictor which includes suspended sediment, compared to the total-load Engelund-Hansen predictor which was entirely treated as bed-load in their model. Fourth, current morphodynamic model simulations generally use only one sediment fraction, while Dastgheib and Roelvink (2010) shows that using multiple fractions in long-term model simulations leads to channel depth reduction, as would a larger bed slope effect, because of bed armoring effects. Finally, lower values for α or α_c, and thus more downslope sediment transport, may be necessary to compensate for subgrid bank erosion processes that usually are not incorporated in the numerical models (Grenfell, 2012; Schuurman et al., 2013).

6. Conclusions

We experimentally tested the effect of a large range in secondary flow intensity and sediment mobility on equilibrium transverse slopes using a rotating annular flume, covering all sediment transport modes and bed states for a wide range of secondary flow intensity.

The resulting trend in slope effect deviates from typical power relations with Shields number and is grainsize-dependent. An increase in secondary flow intensity resulted in an increase in transverse slope until the angle of repose of loose granular sediment was reached. On the other hand, when secondary flows were minimal, the average transverse slope was also minimal. Sediment mobility limited the development of transverse slopes just above the beginning of motion and influenced slope effects by affecting sediment transport mode and bed state. Downslope sediment transport increased when ripples transitioned to dunes in fine sands, and with coarse sand and fine gravel slope effects were minimal when dune height-to-length ratios were low. The presence of dunes had a large influence on flow patterns because of their large height relative to water depth and possibly enhanced secondary flow. Future analysis of flow velocity patterns over large dunes is needed to unravel the exact effect of dunes on transverse bed slope effects and to translate the current results to natural systems.

Downslope sediment transport is significantly lower than in existing transverse slope predictors, especially for coarse sand and fine gravel. Furthermore, the change in slope effect with increasing sediment mobility is higher at low sediment mobility, but significantly lower at higher sediment mobility. Eventually, slope effects become independent of sediment mobility, which is not yet taken into account in current models. The lower downslope sediment transport is in contrast with the tendency to increase slope effects in morphodynamic modeling to compensate for overdeepening of channels. This suggest calibrating the slope effects in current practice is necessary to compensate for other model weaknesses, such as roughness, the choice of sediment transport predictor, or the absence of bank erosion.

Appendix A: Characteristic Normal Flow Velocities

Here, we present the derivation of equation (10) for estimating the characteristic normal flow velocity, which is then calibrated on measured data. We assume that centrifugal forces driving the flow are balanced by frictional forces in the cross section of the flume. The centrifugal force generated by the lid forces water toward the outer bend, which creates a pressure difference that drives the secondary flow and creates an inward-directed bed shear stress. Counterrotation of the floor adds an outward-directed centrifugal force on the flow low in the water column, which decreases the pressure difference over the water column at the outer bend, and thereby decreases the secondary flow and the inward-directed bed shear stress. Therefore, the net-centrifugal force (F_c) is determined by the difference between these two centrifugal forces. We assume that the lid rotation influences the top half of the water column ($H/2$) and the floor rotation affects the bottom half:

$$F_c = \rho \frac{H}{2} W \frac{U_l^2}{r} - \rho \frac{H}{2} W \frac{U_f^2}{r} \tag{A1}$$

This force is balanced by friction exerted along the lid, side walls, and sediment bed:

$$\rho \frac{H}{2} W \frac{U_l^2 - U_f^2}{r} = \tau'_w + \tau'_b + \tau'_l \tag{A2}$$

where τ' = shear stress per unit of downstream length (N/m) exerted on the walls (w), bed (b), and lid (l), respectively.

We consider a cross section of unit length where the friction depends on a measure of both the magnitude of the streamwise flow velocity and the normal flow velocity. Shear stress for any boundary section i is therefore defined as:

$$\tau'_i = \rho c_i L_i u_n u_s \tag{A3}$$

where L = that part of the hydraulic radius on which the shear stress component is exerted (m) and c_i = friction coefficient. As a simple estimate of the characteristic streamwise flow velocity, the average of the lid and floor angular velocity was used as described by equation (9). After inserting the definitions of the shear stress and the streamwise flow velocity into equation (A2), u_n can be isolated:

$$u_n = \frac{HW}{r(c_w(W+H)+c_b W)} \frac{U_l^2 - U_f^2}{(U_l + |U_f|)} \tag{A4}$$

where:

$$\frac{U_l^2 - U_f^2}{(U_l + |U_f|)} = \frac{(U_l - |U_f|)(U_l + |U_f|)}{(U_l + |U_f|)} = U_l - |U_f| \tag{A5}$$

This results in equation (9) after adding the calibration parameters.

The friction coefficient for the rough surface of the bed (c_b) is defined as:

$$c_b = \frac{8}{\left[5.75 \ log\left(\frac{12 r_h}{k_s}\right)\right]^2} \tag{A6}$$

where r_h = hydraulic radius (m) and k_s = Nikuradse roughness height (m). For the flow measurements, we assumed $k_s = 2.5D$. For both the smooth lid and glass walls, smooth wall friction is assumed:

$$c_w = \frac{8}{[5.75 \ log(\frac{12 r_h u_*}{3.3 \nu})]^2} \tag{A7}$$

where u_* = shear velocity (m/s) and ν = viscosity (m^2/s).

Appendix B: Comparison of Transverse Slope Parameters Used in Delft3D

In this section, we describe how the two main methods to calculate sediment transport on transverse bed slopes in Delft3D are related, to make it easier to switch between the two methods when setting up a morphodynamic model. The predictor based on Koch and Flokstra (1981) uses the input parameter A_{sh}, which is

equal to α defined in this paper, while the predictor based on Ikeda (1984) uses the input parameter α_{bn}, which is the inverse of α_c. As described in section 2, the two options differ in the calculation of the resulting transport vector. The predictor based on Koch and Flokstra (1981) does not alter the magnitude of sediment transport, while the predictor based on Ikeda (1984) increases the magnitude as a function of the transverse bed slope. As a result, to be able to compare the two input slope parameters, the predictor based on Koch and Flokstra (1981) has to be corrected for a given slope and sediment mobility. Using equations (6) and (7) with a β of 0.5 it follows that:

$$\alpha_{bn} = \left(A_{sh} \sqrt{\theta_c + \frac{\theta_c}{A_{sh}^2 \theta} \left(\frac{dz}{dy} \right)^2} \right)^{-1} \tag{B1}$$

The resulting relation between α_{bn} and A_{sh} is plotted in Figure 14 for four combinations of transverse slope and sediment mobility.

Acknowledgments
This research was partly supported by Deltares and by the Dutch Technology Foundation STW (grant Vici 016.140.316/13710 to M.G.K., which is part of the Netherlands Organisation for Scientific Research (NWO), and is partly funded by the Ministry of Economic Affairs). This work is part of the PhD research of A.W.B. and MSc research of J.dS. We are grateful to Sander de Vree and Hans Tas of the Environmental Fluid Mechanics Laboratory at the TU Delft for technical support. Discussion with Kees Sloff, reviews by two anonymous reviewers and steer by Associate Editor Christophe Ancey helped to improve the manuscript. The authors contributed in the following proportions to conception and design, data collection, flow modeling, data analysis and conclusions, and manuscript preparation: A.W.B.(50,70,50,60,80)%, J.C.dS.(0,30,0,10,0)%, W.S.J.U.(10,0,40,0,0)%, and M.G.K.(40,0,10,30,20)%. Supporting data are included as one table in the supporting information.

References

Ashley, G. M. (1990). Classification of large-scale subaqueous bedforms: A new look at an old problem-SEPM bedforms and bedding structures. *Journal of Sedimentary Research*, *60*(1), 160–172.

Bennett, S. J., Bridge, J. S., & Best, J. L. (1998). Fluid and sediment dynamics of upper stage plane beds. *Journal of Geophysical Research*, *103*(C1), 1239–1274.

Blondeaux, P., & Vittori, G. (2016). A model to predict the migration of sand waves in shallow tidal seas. *Continental Shelf Research*, *112*, 31–45. https://doi.org/10.1016/j.csr.2015.11.011

Bolla Pittaluga, M., Coco, G., & Kleinhans, M. G. (2015). A unified framework for stability of channel bifurcations in gravel and sand fluvial systems. *Geophysical Research Letters*, *42*, 7521–7536. https://doi.org/10.1002/2015GL065175

Bolla Pittaluga, M., Repetto, R., & Tubino, M. (2003). Correction to channel bifurcation in braided rivers: Equilibrium configurations and stability. *Water Resources Research*, *39*(3), 1323. https://doi.org/10.1029/2003WR002754

Booij, R. (1994). Measurements of the flow field in a rotating annular flume. In *Communications on hydraulic and geotechnical engineering* (Rep. 94-2). Delft, the Netherlands: Department of Civil Engineering, TU Delft.

Booij, R. (2003). Measurements and large eddy simulations of the flows in some curved flumes. *Journal of Turbulence*, *4*(March 2015), 37–41. https://doi.org/10.1088/1468-5248/4/1/008

Bridge, J. S., & Bennett, S. J. (1992). A model for the entrainment and transport of sediment grains of mixed sizes, shapes, and densities. *Water Resources Research*, *28*(2), 337–363.

Crosato, A., & Mosselman, E. (2009). Simple physics-based predictor for the number of river bars and the transition between meandering and braiding. *Water Resources Research*, *45*, W03424. https://doi.org/10.1029/2008WR007242

Dastgheib, A., & Roelvink, J. (2010). Effect of different sediment mixtures on the long-term morphological simulation of tidal basins. In C. Vionnet et al. (Eds.), *River, coastal and estuarine morphodynamics: RCEM 2009* (pp. 913–918). London, UK: Taylor & Francis Group.

Dietrich, W. E., & Smith, J. D. (1984). Bed load transport in a river meander. *Water Resources Research*, *20*(10), 1355–1380. https://doi.org/10.1029/WR020i010p01355

Engelund, F. (1974). Flow and bed topography in channel bends. *Journal of the Hydraulics Division*, *100*(11), 1631–1647.

Engelund, F. (1975). Instability of flow in a curved alluvial channel. *Journal of Fluid Mechanics*, *72*(1), 145–160. https://doi.org/10.1017/S002211207500300X

Fernandez Luque, R., & Van Beek, R. (1976). Erosion and transport of bed-load sediment. *Journal of Hydraulic Research*, *14*(October 2014), 127–144. https://doi.org/10.1080/00221686709499677

Francalanci, S., & Solari, L. (2008). Bed-load transport equation on arbitrarily sloping beds. *Journal of Hydraulic Engineering*, *134*(January), 110–115. https://doi.org/10.1061/(ASCE)0733-9429(2008) 134:1(110)

Francalanci, S., Solari, L., & Toffolon, M. (2009). Local high-slope effects on sediment transport and fluvial bed form dynamics. *Water Resources Research*, *45*, W05426. https://doi.org/10.1029/2008WR007290

Grenfell, M. C. (2012). *Chute channels in large, sand-bed meandering rivers chute channels in large, sand-bed meandering rivers* (PhD thesis). Exeter, UK: University of Exeter.

Hasegawa, K. (1981). Bank-erosion discharge based on a non-equilibrium theory, *Proceedings of the Japan Society of Civil Engineers*, *1981*, 37–50.

Hulscher, S. J. (1996). Tidal-induced large-scale regular bed form patterns in a three-dimensional shallow water model. *Journal of Geophysical Research*, *101*(C9), 20727–20744.

Ikeda, S. (1984). Lateral bed-load transport on side slopes - closure. *Journal of Hydraulic Engineering*, *110*(2), 200–203.

Ikeda, S., & Nishimura, T. (1986). Flow and bed profile in meandering sand silt rivers. *Journal of Hydraulic Engineering*, *112*(7), 562–579. https://doi.org/10.1061/(ASCE)0733-9429(1986)112:7(562)

Kleinhans, M. G., Jagers, H. R. A., Mosselman, E., & Sloff, C. J. (2008). Bifurcation dynamics and avulsion duration in meandering rivers by one-dimensional and three-dimensional models. *Water Resources Research*, *44*, W08454. https://doi.org/10.1029/2007WR005912

Kleinhans, M. G., Leuven, J. R. F. W., Braat, L., & Baar, A. W. (2017). Scour holes and ripples occur below the hydraulic smooth to rough transition of movable beds. *Sedimentology*, *64*(5), 1381–1401. https://doi.org/10.1111/sed.12358

Kleinhans, M. G., Markies, H., De Vet, S. J., in 't Veld, A. C., & Postema, F. N. (2011). Static and dynamic angles of repose in loose granular materials under reduced gravity. *Journal of Geophysical Research*, *116*, E11004. https://doi.org/10.1029/2011JE003865

Kleinhans, M. G., & van den Berg, J. H. (2011). River channel and bar patterns explained and predicted by an empirical and a physics-based method. *Earth Surface Processes and Landforms*, *36*(6), 721–738. https://doi.org/10.1002/esp.2090

Kisling-Moller, J. (1993). Bedform migration and related sediment transport in a meander bend. In M. Marzo and C. Puigdefábregas (Eds.), *Alluvial sedimentation, Special Publication 17 of the IAS* (Vol. 66, 51 p.). Oxford, UK: Blackwell Publishing Ltd. https://doi.org/10.1002/9781444303995.ch5

Koch, F., & Flokstra, C. (1981). Bed level computations for curved alluvial channels. In *19th International association for hydraulic research congress* (Vol. 240, 10 p.). Delft, the Netherlands: Delft Hydraulics Laboratory.
Leuven, J. R. F. W., Kleinhans, M. G., Weisscher, S. A. H., & Vegt, M. V D. (2016). Tidal sand bar dimensions and shapes in estuaries. *Earth Science Reviews*, *161*, 204–223. https://doi.org/10.1016/j.earscirev.2016.08.004
Odgaard, A. J. (1981). Transverse bed slope in alluvial channel bends, *Journal of the Hydraulics Division, Proceedings of the American Society of Civil Engineers*, 107, 1577–1594.
Parker, G., Seminara, G., & Solari, L. (2003). Bed load at low Shields stress on arbitrarily sloping beds: Alternative entrainment formulation. *Water Resources Research*, *39*(7), 1183. https://doi.org/10.1029/2001WR001253
Ruessink, B. G., Kuriyama, Y., Reniers, A. J. H. M., Roelvink, J. A., & Walstra, D. J. R. (2007). Modeling cross-shore sandbar behavior on the timescale of weeks. *Journal of Geophysical Research*, *112*, F03010. https://doi.org/10.1029/2006JF000730
Schramkowski, G. P., Schuttelaars, H. M., & De Swart, H. E. (2002). The effect of geometry and bottom friction on local bed forms in a tidal embayment. *Continental Shelf Research*, *22*(11–13), 1821–1833. https://doi.org/10.1016/S0278-4343(02)00040-7
Schuurman, F. (2015). *Bar and channel evolution in meandering and braiding rivers using physics-based modeling* (PhD thesis). Utrecht, the Netherlands: Utrecht University.
Schuurman, F., Marra, W. A., & Kleinhans, M. G. (2013). Physics-based modeling of large braided sand-bed rivers: Bar pattern formation, dynamics, and sensitivity. *Journal of Geophysical Research: Earth Surface*, *118*, 2509–2527. https://doi.org/10.1002/2013JF002896
Sekine, M., & Parker, G. (1992). Bed-load transport on transverse slope. *Journal of Hydraulic Engineering*, *118*(4), 513–535.
Seminara, G., Solari, L., & Parker, G. (2002). Bed load at low Shields stress on arbitrary sloping beds: Failure of the Bagnold hypothesis. *Water Resources Research*, *38*(11), 1249. https://doi.org/10.1029/2001WR000681
Seminara, G., & Turbino, M. (2001). Sand bars in tidal channels. Part 1. Free bars. *Journal of Fluid Mechanics*, *440*(2001), 49–74.
Sieben, J., & Talmon, A. M. (2011). Bed-load transport in obliquely dune-covered riverbeds. *Journal of Hydraulic Research*, *493*, (November 2012), 317–324. https://doi.org/10.1080/00221686.2011. 566252
Sloff, K., & Mosselman, E. (2012). Bifurcation modelling in a meandering gravel-sand bed river. *Earth Surface Processes and Landforms*, *37*(14), 1556–1566. https://doi.org/10.1002/esp.3305
Soulsby, R., & Whitehouse, R. (1997). Threshold of sediment motion in coastal environments. In *Pacific Coasts and Ports' 97: Proceedings of the 13th Australasian Coastal and Ocean Engineering Conference and the 6th Australasian Port and Harbour Conference* (Vol. 1, p. 145). Christchurch, New Zealand: Centre for Advanced Engineering, University of Canterbury.
Struiksma, N., Olesen, K. W., Flokstra, C., & De Vriend, H. J. (1985). Bed deformation in curved alluvial channels. *Journal of Hydraulic Research*, *23*(1), 57–79. https://doi.org/10.1080/00221688509499377
Talmon, A., Struiksma, N., & Van Mierlo, M. (1995). Laboratory measurements of the direction of sediment transport on transverse alluvial-bed slopes. *Journal of Hydraulic Research*, *33*(4), 495–517. https://doi.org/10.1080/00221689509498657
Talmon, A. M., & Wiesemann, J. (2006, November 1–3). Influence of grain size on the direction of bed-load transport on transverse sloping beds In H. J. Verheij & G. J. Hoffmans (Eds.), *Proceedings Third International Conference on Scour and Erosion* (pp. 632–639). Amsterdam, the Netherlands: CURENT.
Ten Brinke, W., Wilbers, A., & Wesseling, C. (1999). Dune growth, decay and migration rates during a large-magnitude flood at a sand and mixed sand–gravel bed in the Dutch Rhine river system. *Fluvial Sedimentology*, *VI*, 15–32.
Van Bendegom, L. (1947). Enige beschouwingen over riviermofologie en rivierverbetering. *De Ingenieur*, *59*(4), 1–11.
Van den Berg, J., & Van Gelder, A. (1993). A new bedform stability diagram, with emphasis on the transition of ripples to plane bed in flows over fine sand and silt. In M. Marzo and C. Puigdefábregas (Eds.), *Alluvial Sedimentation, Special Publication*. (Vol. 17, pp. 11–21). Oxford, UK: Blackwell Publishing Ltd. https://doi.org/10.1002/9781444303995.ch2
Van der Wegen, M., & Roelvink, J. A. (2012). Reproduction of estuarine bathymetry by means of a process-based model: Western Scheldt case study, the Netherlands. *Geomorphology*, *179*, 152–167. https://doi.org/10.1016/j.geomorph.2012.08.007
Van Rijn, L. C. (1984a). Sediment transport, part i: Bed load transport. *Journal of Hydraulic Engineering*, *110*(10), 1431–1456.
Van Rijn, L. C. (1984b). Sediment transport, part iii: Bed forms and alluvial roughness. *Journal of Hydraulic Engineering*, *110*(12), 1733–1754.
Van Rijn, L. C. (1984c). Sediment pick-up functions. *Journal of Hydraulic Engineering*, *110*(10), 1494–1502.
Van Rijn, L. C. (1993). *Principles of sediment transport in rivers, estuaries and coastal seas*. Amsterdam, the Netherlands: Aqua Publications.
Venditti, J. G., Church, M., & Bennett, S. J. (2005). On the transition between 2d and 3d dunes. *Sedimentology*, *52*(6), 1343–1359.
Wiesemann, J.-U., Mewis, P., & Zanke, U. C. E. (2006). Downslope transport (transverse sediment transport). In *Third Chinese-German joint symposium in coastal and ocean engineering*. Tainan, Taiwan: National Cheng Kung.
Yang, S.-H., Im, I.-T., Hwang, K.-N., Cho, Y.-S., & Ryu, H.-R. (2015). A numerical study on optimal rotation ratio and bottom shear stress in the counter-rotation mode of an annular flume. *Journal of Hydro-Environment Research*, *9*(4), 473– 481. https://doi.org/10.1016/j.jher.2015.02.002